The topology of lymphotoxin β receptor accumulated upon endolysosomal dysfunction dictates the NF-κB signaling outcome

Magdalena Banach-Orłowska[1]†, Kamil Jastrzębski[1]†, Jarosław Cendrowski[1], Małgorzata Maksymowicz[1], Karolina Wojciechowska[1], Michał Korostyński[2], Dimitri Moreau[3], Jean Gruenberg[3], Marta Miaczynska[1]*

[1] Laboratory of Cell Biology, International Institute of Molecular and Cell Biology, 02-109, Warsaw, Poland

[2] Department of Molecular Neuropharmacology, Institute of Pharmacology Polish Academy of Sciences, 31-343, Krakow, Poland

[3] Department of Biochemistry, University of Geneva, 1211, Geneva, Switzerland

* Corresponding author. Tel: +48 22 597 07 25; E-mail: miaczynska@iimcb.gov.pl

† These authors contributed equally to this work

Summary statement

Sequestration of LTβR in intraluminal vesicles of endosomes upon depletion of HOPS components or Rab7 precludes NF-κB signaling, whereas LTβR accumulation on the outer endosomal membrane after ESCRT depletion promotes signaling.

Abstract

Cytokine receptors, such as tumor necrosis factor receptor I (TNFRI) and lymphotoxin β receptor (LTβR), activate inflammatory NF-κB signaling upon stimulation. We previously demonstrated that depletion of ESCRT components leads to endosomal accumulation of TNFRI and LTβR, and their ligand-independent signaling to NF-κB. Here, we studied if other perturbations of the endolysosomal system could trigger intracellular accumulation and signaling of ligand-free LTβR. While depletion of CORVET had no effect, knockdown of HOPS or Rab7, or pharmacological inhibition of lysosomal degradation, caused endosomal accumulation of LTβR and its increased interactions with TRAF2/TRAF3 signaling adaptors. However, the NF-κB pathway was not activated under these conditions. We found that knockdown of HOPS or Rab7 led to LTβR sequestration in intraluminal vesicles of endosomes, thus precluding NF-κB signaling. This was in contrast to LTβR localization on the outer endosomal membrane after ESCRT depletion that was permissive for signaling. We propose that the inflammatory response induced by intracellular accumulation of endocytosed cytokine receptors critically depends on the precise receptor topology within endosomal compartments.

Introduction

Among other functions, endocytosis serves to maintain homeostasis of the plasma membrane and to downregulate receptors that perform signaling functions. The targeting of cell surface proteins for lysosome degradation is initiated at the plasma membrane by ubiquitin conjugation. Subsequently, ubiquitylated cargo is internalized into endosomes and recognized by subunits of the endosomal sorting complexes required for transport (ESCRT) (Christ et al., 2017; Frankel and Audhya, 2018). ESCRTs assemble on endosomal membranes and also drive the formation of intraluminal vesicles (ILVs) which contain the downregulated cargo. In parallel, early endosomes marked with Rab5 mature into Rab7-positive late endosomes in a process controlled by Rab5-to-Rab7 conversion (Huotari and Helenius, 2011; Poteryaev et al., 2010; Rink et al., 2005; Scott et al., 2014). Finally, late endosomes fuse with lysosomes, where cargo is degraded. However, it is not clear how cargo sorting for degradation is coordinated with endosomal membrane dynamics. In the endosomal system, docking/fusion depends on two tethering complexes: class C core vacuole/endosome tethering (CORVET), and homotypic fusion and protein sorting (HOPS), which in yeast are recruited by Rab5 and Rab7, respectively (Balderhaar and Ungermann, 2013; Spang, 2016). In mammalian cells, HOPS does not interact with Rab7 but is recruited to membranes via interaction with Arl8b and RILP (Khatter et al., 2015; Lin et al., 2014). Both CORVET and HOPS complexes are composed of six subunits, with four (Vps11, Vps16, Vps18, and Vps33A) being shared between them. The complexes differ by two subunits: Vps3 (also known as TGFBRAP1, TRAP1) and Vps8 in CORVET, versus Vps39 and Vps41 in HOPS (Markgraf et al., 2009; Peplowska et al., 2007; Price et al., 2000).

Endocytic internalization and trafficking can regulate signal transduction of plasma membrane receptors in multiple ways. They include termination of signaling by lysosomal degradation of receptors but also maintenance of signaling by retention of active receptors on endosomes (Barbieri et al., 2016; Miaczynska, 2013; Szymanska et al., 2018; Villasenor et al., 2016). While our knowledge of mechanisms linking trafficking and signaling comes mostly from research on receptor tyrosine kinases or G protein-coupled receptors, less is known about cytokine receptors of the tumor necrosis factor receptor (TNFR) superfamily (Cendrowski et al., 2016). Of the latter class, we focused on lymphotoxin β receptor (LTβR), which is activated by membrane-bound ligands lymphotoxin α1β2 or LIGHT (Remouchamps et al., 2011). In contrast to a relatively broad expression pattern of the receptor, the expression of its ligands is restricted to lymphocytes (B, T and NK cells). Upon stimulation,

LTβR recruits cytoplasmic TNFR-associated factor (TRAF) adaptors (Kim et al., 2005; Nakano et al., 1996; VanArsdale et al., 1997) and activates both the canonical and non-canonical NF-κB pathways (Dejardin et al., 2002; Muller and Siebenlist, 2003). Further downstream, the canonical pathway is driven by degradation of IκBα inhibitor, followed by phosphorylation and nuclear translocation of NF-κB transcription factor RelA. The non-canonical branch involves processing of p100 NF-κB precursor to a transcriptionally active p52 (Zhang et al., 2017).

While the signaling pathways of LTβR are well established, its trafficking routes are less studied. Ligand-induced LTβR was reported to undergo dynamin-mediated internalization that was linked to the activation of non-canonical NF-κB signaling (Ganeff et al., 2011). However, most cell types do not express LTβR ligands. We have recently shown that at steady state HEK 293 cells contain an intracellular pool of ligand-free LTβR that largely overlaps with endosomal markers EEA1 or LAMP1, with over 30% colocalization with either marker (Maminska et al., 2016). Importantly, accumulation of ligand-free LTβR on endosomes markedly increases upon depletion of ESCRT-I components that interferes with cargo sorting into ILVs and its lysosome targeting. Under these conditions, local oligomerization and activation of LTβR trigger canonical and non-canonical NF-κB signaling from endosomes in a ligand-independent manner (Maminska et al., 2016). However, it remained unclear whether other perturbations of the endosomal system also lead to an increased intracellular accumulation of LTβR as well as inflammatory NF-κB signaling in cells that do not express LTβR ligands. In this study, we investigated whether dysfunction of the other endosomal complexes CORVET and HOPS, involved in endosome maturation, affected trafficking and signaling of ligand-free LTβR. We show that depletion of Rab7 or HOPS caused accumulation of the receptor on endosomes but, in contrast to ESCRT knockdown, without induction of the NF-κB pathway. We propose that different effects of ESCRT or HOPS depletion on inflammatory signaling result from the different topology of ligand-free LTβR accumulated in endosomes under both conditions.

Results

HOPS but not CORVET regulates intracellular trafficking of LTβR.

To assess the involvement of CORVET and HOPS complexes in trafficking of ligand-free LTβR, we depleted their two common core subunits, Vps16 and Vps18 (Fig. 1A-E), and checked intracellular distribution of LTβR in HeLa cells using confocal microscopy. When compared to control cells (transfected with non-targeting siRNAs), cells deprived of either subunit exhibited stronger vesicular staining of LTβR (Fig. 1A). We quantitatively analyzed the images with respect to integral fluorescence intensity of EEA1-, LAMP1- or LTβR-positive vesicles as the parameter that represents the amount of a particular protein localized to vesicular structures (Fig. 1B,C). Moreover, for LTβR we calculated its concentration per vesicle (represented by mean of integral fluorescence intensity) (Fig. 1C) and colocalization of the receptor with endosomal markers upon Vps16 or Vps18 depletion (Fig. 1D). In general, quantitative image analysis revealed no substantial changes in the integral intensity of EEA1- or LAMP1-positive vesicles. Importantly, both total amounts and concentration of LTβR per vesicle were increased under these conditions (Fig. 1C), although its colocalization with early or late endosome markers was not affected (Fig. 1D). Nevertheless, these data allowed concluding that the disruption of CORVET and/or HOPS complexes led to the vesicular accumulation of LTβR.

To discriminate which of the two complexes was required for the regulation of LTβR trafficking we knocked down expression of their specific subunits. We found that neither the general distribution of LTβR nor its amounts and concentration on endosomes were affected upon depletion of CORVET subunits Vps3 and Vps8 (Fig. S1A,B). Their silencing was efficient (Fig. S1C) and led to increased colocalization of transferrin with EEA1 (Fig. S1D), as previously reported (Perini et al., 2014). We concluded that CORVET was functional in our cellular model, however, it was dispensable for LTβR sorting.

Next, we investigated whether HOPS was involved in intracellular transport of LTβR. To this end, we depleted the unique subunits of this complex, Vps39 and Vps41, as well as another common HOPS/CORVET subunit Vps11 (Fig. 2A-E). Integral intensity of EEA1- but not LAMP1-positive endosomes was increased in these cells (Fig. 2B). In agreement with the data from Vps16 and Vps18 depleted cells (Fig. 1A,C), we also found a higher endosomal accumulation of LTβR upon Vps11, Vps39 and Vps41 silencing (Fig. 2A,C). Interestingly,

colocalization of LTβR on vesicles positive for both LAMP1 and EEA1 was increased (Fig. 2D), suggesting that LTβR accumulates on aberrant endosomes bearing simultaneously both markers. The observed change in LTβR cellular distribution after depletion of Vps39, Vps41 or Vps11 was not accompanied by a significant change in LTβR abundance, as measured by immunoblotting (Fig. 2F). This implies that LTβR is re-localized in cells upon depletion of HOPS components.

To exclude possible off-target effects of siRNA, we prepared HeLa cell lines with depletion of Vps39 or Vps41 using the CRISPR/Cas9 approach. For each protein we used two independent single guide RNA (sgRNA) sequences. Parental HeLa cells were employed as a control. Similarly to siRNA for Vps39 and Vps41, we observed changes in the distribution of LTβR and endosomal markers (Fig. S2A-C). The values of both integral and mean fluorescence intensity of LTβR were higher (Fig. S2C) and colocalization of the receptor with LAMP1 and EEA1 was increased in CRISPR-modified cells (Fig. S2D), as it was upon siRNA-mediated HOPS depletion (Fig. 2C,D) These effects were clearly measureable despite the modest efficiency of depletion mediated by sgRNA which was likely due to heterogeneity in the investigated pools of cells (Fig. S2E,F).

Altogether, these data indicate that trafficking of ligand-free LTβR engages the HOPS tethering complex but not CORVET. These observations also suggest that although the two complexes share a common core, their functions can be uncoupled, with CORVET playing possibly a more specialized role in the transport of certain cargoes.

Rab7 regulates trafficking and degradation of LTβR.

The HOPS complex in yeast is recruited to endosomal membranes by Rab7 (Balderhaar and Ungermann, 2013; Spang, 2016). In mammalian cells, the role of Rab7 in this process is still unclear (Guerra and Bucci, 2016). However, Rab7 is a key regulator of transition from early to late endosomes and could potentially regulate LTβR trafficking. To evaluate this, we investigated the intracellular distribution of the receptor by confocal microscopy in cells transfected with two independent siRNAs (Fig. 3A-D) or one shRNA targeting Rab7 (Fig. S3A-C). We found that Rab7 depletion affected the distribution of LTβR (Fig. 3A,C, S3A,B) and EEA1 (Fig. 3A,B). Quantitative analysis of images revealed that both the amounts and the concentration of LTβR on vesicles were increased (Fig. 3C; S3B). Moreover, similarly to HOPS depletion, Rab7 removal resulted in higher amounts of EEA1

on endosomes without affecting LAMP1-marked vesicles (Fig. 3A,B) and led to increased colocalization of the receptor with EEA1 and LAMP1 (Fig. 3D).

To further confirm the role of Rab7 as a regulator of LTβR trafficking we performed rescue experiments using overexpression of canine Rab7 tagged with HA. As a control we used an empty pcDNA3 plasmid with HA. As expected, in cells transfected with Rab7_2 siRNA and Rab7 plasmid (resistant to this siRNA) we could observe expression of canine Rab7 protein visualized by HA staining (Fig. 3E) and significant reduction of the vesicular accumulation of LTβR in comparison to that measured in cells cotransfected with Rab7_2 siRNA and empty pcDNA plasmid with HA (Fig. 3F). As additional control, we saw no expression of HA-Rab7 in cells transfected with Rab7_1 siRNA (fully matching the dog Rab7 sequence) and high endosomal LTβR accumulation remained unchanged (Fig. 3E,F).

As the analysis of microscopic data showed elevated amounts and concentration of the receptor on vesicles in Rab7-depleted cells, we measured total abundance of LTβR by immunoblotting. In contrast to the depletion of HOPS components, Rab7 knockdown caused statistically significant increase in total receptor levels (Fig. 3G), implying that LTβR degradation was impaired under these conditions.

Cumulatively, our findings suggest that ligand-free LTβR can be constitutively endocytosed and sorted to lysosomes in a process involving Rab7. While the requirement for Rab7 appears to be critical for efficient LTβR degradation, depletion of HOPS (Fig. 2F) or ESCRT (Maminska et al., 2016) does not change abundance of LTβR. This may point to the existence of some compensatory or by-pass mechanisms for elimination of excess LTβR (e.g. via alternative routes to lysosomal degradation) when these complexes are dysfunctional.

Rab7- and Vps11-depleted cells show increased LTβR-TRAF association that does not activate the NF-κB pathway.

The increased accumulation of LTβR on endosomes upon depletion of Rab7 or HOPS components prompted us to test whether the receptor is in an active state and induces NF-κB signaling from endosomes, as it does upon ESCRT depletion (Maminska et al., 2016). A prerequisite for the NF-κB pathway activation is the recruitment of TRAF adaptor proteins to oligomerized LTβR that occurs upon ligand stimulation, or, as we previously demonstrated, upon ESCRT dysfunction in the absence of ligands (Maminska et al., 2016). We thus measured the interactions between LTβR and TRAF2/TRAF3 proteins using

immunoprecipitation from lysates of cells transfected with control siRNAs or siRNAs targeting Rab7, or a representative HOPS subunit Vps11. Fig. 4A shows greatly increased amounts of TRAF2 and TRAF3 co-immunoprecipitated with LTβR in cells with knockdown of Rab7 or Vps11. Since Rab7-deprived cells contain more LTβR, we quantified the ratio of co-immunoprecipitated TRAF2 to immunoprecipitated LTβR. Also after such normalization, there were significantly more LTβR-TRAF2 complexes upon Rab7 or Vps11 knockdown than in control cells (graph in Fig. 4A). In addition, total TRAF2 or TRAF3 levels were not changed upon Rab7 or Vps11 knockdown (Fig. S4A).

These results suggested that in cells depleted of Rab7 or HOPS components, LTβR is activated and able to trigger NF-κB signaling. We thus assessed the activity of both the canonical and non-canonical branches of the NF-κB pathway by measuring the status of their effector proteins. Surprisingly, Rab7 or HOPS depletion had no effect on the phosphorylation of RelA, the levels of the pathway inhibitor IκBα (hallmarks of the canonical branch), or p100 processing into active p52 (a hallmark of the non-canonical branch) (Fig. 4B,C). In contrast, knockdown of the ESCRT-I component Vps28 activated the NF-κB pathway (Fig. 4D), as previously shown (Maminska et al., 2016).

 Since it is known that LTβR can also induce JNK signaling (Chang et al., 2002; Kim et al., 2005) we examined its status upon depletion of Rab7, HOPS or ESCRT but did not detect active phosphorylated form of JNK (Fig. S4B,C), although JNK signaling could be induced in HeLa cells by addition of agonistic antibody for LTβR (Fig. S4D). We also monitored phosphorylation of Akt and Erk1/2, which are commonly activated in response to the stimulation of membrane receptors. We found that depletion of HOPS components or Rab7 did not induce these signaling pathways (Fig. S4B,C). Increased phosphorylation of Erk1/2 was only observed upon ESCRT depletion (Fig. S4C), that was previously shown to enhance EGF-induced Erk1/2 activation (Brankatschk et al., 2012).

In parallel to biochemical analyses, we examined the effect of HOPS or Rab7 depletion at the transcriptional level. qRT-PCR analysis confirmed that there was no activation of selected NF-κB target genes (Fig. S5A). Increased *TNF* or *RELB* expression observed for single siRNAs (Vps11_1, Rab7_2) was not reproduced by other reagents and probably reflected unspecific off-target effects. In contrast, Vps28 depletion potently induced expression of 4 out of 6 selected target genes, *IL8, TNF, ICAM1* and *NFKBIA* (Fig. S5B), in line with our biochemical analysis (Fig. 4D) and our previous study (Maminska et al., 2016). Altogether, these data show that in HeLa cells the NF-κB pathway was not activated upon

Rab7 or HOPS depletion, despite robust interactions of LTβR with its signaling TRAF adaptors.

Since we had previously shown that the NF-κB pathway was very strongly activated upon ESCRT silencing in HEK 293 cells (Maminska et al., 2016), we repeated our experiments in these cells as an additional control. We again found that knockdown of HOPS components did not affect the transcription of NF-κB target genes (Fig. S5C), while depletion of Vps28 induced a very potent inflammatory transcriptional response (Fig. S5D).

Finally, to assess whether instead of NF-κB, other intracellular signaling pathways are affected by HOPS knockdown, we analyzed the transcriptome of HEK 293 cells depleted of Vps11, Vps39 or Vps41. We found no pronounced changes in a general expression profile of HEK 293 cells transfected with siRNAs targeting the HOPS components (Fig. S5E). We did not detect any transcriptional signature of particular signaling pathways among 108 significantly up-regulated genes, which encode mainly plasma membrane or secreted proteins. Hence, the lack of a signaling response after depletion of Vps11, Vps39 or Vps41 in both HeLa and HEK 293 cell lines demonstrates that the endosomal accumulation of LTβR is clearly not sufficient to activate NF-κB signaling. Furthermore, in contrast to ESCRT dysfunction (Brankatschk et al., 2012; Maminska et al., 2016), inactivation of HOPS has no major impact on the cellular transcriptional program.

Inhibition of lysosomal degradation leads to endosomal accumulation of LTβR and its increased binding to TRAF proteins without activating the NF-κB pathway.

To further corroborate our findings, we employed a pharmacological approach to inhibit lysosomal degradation and check its impact on LTβR trafficking and activation. To this end, we used chloroquine, which prevents acidification of endosomal compartments and thus inhibits the activity of lysosomal enzymes. Chloroquine treatment of HeLa cells did not change integral intensity of EEA1 or LAMP1 vesicles (Fig. 5A,B), but significantly increased both amounts and concentration of LTβR on vesicles which predominantly colocalized with LAMP1 (Fig. 5A,C,D). This may indicate that under these conditions, the receptor accumulates in late endosomes/lysosomes, rather than in aberrant vesicles marked with LAMP1 and EEA1 that occurs upon depletion of HOPS or Rab7. We verified by immunoblotting analyses that the total levels of LTβR were increased (Fig. 5E) pointing to the impairment of lysosomal degradation of the receptor in chloroquine-treated cells.

Importantly, NF-κB signaling was not activated under these conditions (Fig. 5E), although the receptor strongly interacted with TRAF proteins (Fig. 5F). These data demonstrate that the chloroquine treatment phenocopies the effects of Rab7 depletion. In both cases, inhibition of lysosomal degradation results in the accumulation of LTβR bound to its signaling adaptor without induction of the NF-κB pathway.

The topology of LTβR accumulated on EEA1-positive endosomes in cells depleted of HOPS or defective in lysosomal degradation is different than in ESCRT-depleted cells.

Next, we investigated why the NF-κB signaling outcome is different in cells depleted of ESCRT-I versus HOPS/Rab7. In both cases, LTβR accumulates intracellularly on endosomes in an active state, as it is strongly associated with its signaling TRAF adaptors. In ESCRT-depleted cells, this leads to pronounced NF-κB activation and inflammatory signaling, while upon HOPS/Rab7 knockdown (or chloroquine treatment) signaling is not induced. We hypothesized that different suborganellar localization of LTβR within endosomes may account for these differences. Specifically, as ESCRTs regulate the formation of ILVs on endosomes, we predicted that ESCRT-I depletion would lead to the accumulation of LTβR on the outer, limiting membrane of enlarged endosomes. In this case, the intracellular part of the receptor would be exposed to the cytoplasm and could interact with components of the NF-κB pathway. In contrast, in HOPS/Rab7-depleted cells or in cells treated with chloroquine, LTβR would not be degraded but sequestered inside properly formed ILVs, from where it could not transduce NF-κB signaling to the cytoplasm.

To verify this hypothesis, we investigated the topology of LTβR on endosomes using Airyscan microscopy that provides higher resolution images when compared to regular confocal microscopy. In ESCRT-depleted cells, LTβR was found on the outer membrane of enlarged vesicles, where it colocalized with EEA1, which resides on the cytoplasmic leaflet of the endosomal membrane (Fig. 6A). Upon HOPS depletion, the accumulated receptor localized inside the lumen of enlarged endosomes and showed only limited colocalization with EEA1 (Fig. 6A). A similar phenotype was observed in cells with Rab7 knockdown (Fig. 6A) or treated with chloroquine (Fig. 6B).

To further investigate the differences in the endosomal topology of LTβR in ESCRT- versus HOPS/Rab7-depleted cells, cellular membranes were differentially solubilized with detergents. A short treatment with low concentration of digitonin should permeabilize only

the plasma membrane, while saponin should permeabilize both the plasma membrane and endosomal membranes (Malerod et al., 2007; Villasenor et al., 2016). Therefore, epitopes located inside the lumen of endosomes should be inaccessible for antibodies in cells permeabilized with digitonin but well detected upon saponin treatment. We combined these treatments with the use of antibodies that recognize the cytoplasmic (intracellular) or the luminal (extracellular) part of LTβR (mouse and goat antibodies, respectively). We expected that if LTβR is present predominantly at the outer endosomal membrane, its cytoplasmic tail but not its luminal part should be readily detected after digitonin permeabilization. In turn, LTβR sequestered in ILVs should be largely protected from detection by both antibodies after digitonin treatment. In all cases, saponin permeabilization should allow for efficient detection of both LTβR epitopes. As an additional control, we used an antibody against the cytoplasmic C-terminus of LAMP1, as its staining should not differ in cells treated with digitonin or saponin.

After digitonin permeabilization of ESCRT-depleted cells, we could detect the cytoplasmic tail of LTβR, but not its luminal part (Fig. S6). This indicated that LTβR localized preferentially on the outer membrane of endosomes. By contrast, after digitonin treatment of HOPS- or Rab7-depleted cells, both parts of LTβR were poorly detected (Fig. S6). This argued that both LTβR epitopes were protected inside endosomes. We then quantified the integral intensity of LTβR signal derived from its intracellular tail after digitonin and saponin permeabilization. The comparison of these two values allowed us to estimate the fraction of LTβR exposed on the outer membrane of endosomes. We observed that this fraction was significantly lower in HOPS- or Rab7-depleted cells, consistent with the localization of LTβR in ILVs, when compared to ESCRT knockdown (Fig. 6C). Taken together, these results show that the intra-endosomal topology of accumulated LTβR is different in cells depleted of various regulators of endocytic trafficking. This different suborganellar localization of the receptor further determines its ultimate signaling outcome.

Discussion

Overall, the findings presented in this study shed light on the still poorly characterized trafficking of LTβR and the regulation of ligand-independent NF-κB signaling. We observed strong intracellular accumulation of LTβR on endocytic structures upon depletion of endosomal sorting/tethering complexes or upon chemical inhibition of lysosomal

degradation. This indicates that the receptor is constitutively internalized, even in the absence of its ligands. Our present and previous studies (Maminska et al., 2016) suggest that internalized LTβR is trafficked through multivesicular endosomes, formed in an ESCRT-dependent manner, that then mature and fuse with lysosomes in a process regulated by Rab7 and HOPS. Since results obtained in yeast indicate that CORVET and HOPS complexes act sequentially during endosomal transport (Balderhaar and Ungermann, 2013), we were surprised to see no effect of CORVET depletion on LTβR trafficking. Experimental data on the function of mammalian CORVET is still limited, however recently it has been implicated in integrin recycling (Jonker et al., 2018). Thus, we cannot rule out that upon CORVET deficiency, fusion of early endosomes can be mediated by other endocytic machineries (Balderhaar et al., 2013). It is also possible that distinct subpopulations of early endosomes harboring various cargoes can cooperate with specific tethering complexes. Moreover, different effects of ESCRT and HOPS depletion on LTβR trafficking and signaling also argue that ESCRT-dependent ILV formation occurs in parallel to and can be uncoupled from HOPS-mediated Rab conversion. While normally these two processes are coordinated in time to ensure proper endosomal transport, their mechanisms are independent and can be selectively perturbed with different consequences for cargo trafficking and, possibly, signaling.

With respect to the signaling of LTβR, we discovered that its intraendosomal sequestration in ILVs upon Rab7/HOPS depletion prevents the transmission of signals to activate the NF-κB pathway, although the receptor is in an active state, bound to the TRAF adaptors (Fig. 6D). This is in contrast to the accumulation of LTβR-TRAF complexes on the outer membrane of endosomes upon ESCRT depletion that activates NF-κB signaling (Maminska et al., 2016). The concept of intraendosomal sequestration of signaling molecules was already proposed for the canonical Wnt pathway, where a negative regulator GSK3β was enclosed in ILVs upon ligand stimulation, thus allowing for signal transduction (Dobrowolski et al., 2012; Taelman et al., 2010). In our case, active LTβR-TRAF complexes, formed in the absence of ligand stimulation, are incorporated into ILVs that inhibits signaling. Previous studies reported that TRAF2 can indeed undergo lysosomal degradation upon ligand-induced NF-κB activation (Varfolomeev et al., 2012; Vince et al., 2008). However, our findings refer to ligand-free conditions and in this context, it was surprising to detect robust LTβR-TRAF interaction upon inhibition of lysosomal degradation by Rab7 depletion or chloroquine treatment (Fig. 4A, 5F). This poses a question of where and when this association forms, as it

requires recruitment of TRAFs from the cytoplasm and is expected to occur before the incorporation of LTβR into ILVs. In control cells, we detected limited binding between LTβR and TRAFs. This may suggest that in the steady-state a certain proportion of LTβR could be activated (e.g. due to stochastic or regulated clustering and proximity-driven oligomerization) and recruit TRAFs at the plasma membrane and/or endosomes. However, due to constitutive internalization of the receptor, such LTβR-TRAF complexes would be efficiently enclosed inside ILVs and subsequently degraded, thereby preventing their signaling. Now we show that trafficking deficiencies can lead to the build-up of LTβR-TRAF complexes which can signal to NF-κB if accumulated on the outer membrane of endosomes and exposed to the cytoplasm (upon ESCRT depletion), or cannot signal when incorporated into ILVs (upon Rab7/HOPS depletion or chloroquine treatment) (Fig. 6D).

Generally, our study demonstrates that endosomal sorting and transport represents a regulatory mechanism to limit NF-κB signaling or prevent its spurious induction in the absence of exogenous stimulation. On the other hand, NF-κB activation initiated by LTβR and other cytokine receptors accumulated on endosomes upon trafficking defects can be considered as a signal of organellar dysfunction. We discovered that such intracellularly induced inflammatory response critically depends on the exact endosomal sorting defect and the resulting topology of cytokine receptors within the endosomal compartments.

Materials and Methods

Cell culture

HeLa, HEK 293 and HEK 293T cells were purchased from ATCC and later authenticated as required. HeLa cells were maintained in modified Eagle's medium (MEM) high glucose, HEK 293 and HEK 293T cells were grown in Dulbecco's modified Eagle's medium (DMEM) high glucose (Sigma-Aldrich), both media supplemented with 10% fetal bovine serum (FBS) and 2 mM L-glutamine (Sigma-Aldrich). Cells were routinely tested for mycoplasma contamination. Chloroquine (Sigma-Aldrich) was used at 100 µM concentration for 20 h. For analysis of transferrin and EGF internalization, HeLa cells were serum-starved overnight and then stimulated for 15 min in serum-free medium with 25 µg/ml transferrin labeled with Alexa Fluor 647 (T23366) and 100 ng/ml biotinylated EGF complexed to Alexa Fluor 555 streptavidin (E35350) from ThermoFisher Scientific.

Antibodies

Primary antibodies used for Western blotting were: rabbit anti-Vps11 (19140-1-AP, 1:600) and anti-Vps41 (13869-1-AP, 1:200) from ProteinTech; rabbit anti-GAPDH (sc-25778, 1:2000), rabbit anti-TRAF3 (sc-949, 1:500) and goat anti-LTβR (sc-8375, 1:500) from Santa Cruz Biotechnology; mouse anti-vinculin (V9131, 1:5000) from Sigma-Aldrich; rabbit anti-p100/p52 (4882S), rabbit anti-phospho-Akt (9271S), mouse anti-Akt (2920S), rabbit anti-phospho-Erk1/2 (9101S), mouse anti-Erk1/2 (9107S), mouse anti-IκBα (4814S), mouse anti-phospho-JNK (9255S), rabbit anti-JNK (9252S), rabbit anti-phospho-RelA (3033), mouse anti-RelA (6956S) and rabbit anti-Rab7 (9367) from Cell Signaling Technology, all diluted 1:1000; rabbit anti-Vps28 (ab167172, 1:1000) from Abcam; mouse anti-TRAF2 (558890, 1:1000) from BD Biosciences.

Primary antibodies used for immunofluorescence were: rabbit anti-EEA1 (ALX-210-239, 1:400) from Enzo Life Sciences; rabbit anti-HA (sc-805, 1:200) from Santa Cruz Biotechnology; agonistic goat anti-LTβR (AF629, IF 1:200) from R&D Systems; mouse anti-LTβR (H00004055-B01P, 1:200) from Abnova, rabbit anti-LAMP1 (L-1418, 1:400) from Sigma-Aldrich, and mouse anti-LAMP1 (H4A3, IF 1:800) developed by J.T. August and J.E.K. Hildreth from the Developmental Studies Hybridoma Bank developed under the auspices of the NICHD and maintained by the University of Iowa, Department of Biology, Iowa City, Iowa, USA.

Secondary horseradish peroxidase-conjugated anti-mouse (111-035-062), anti-rabbit (111-035-144) and anti-goat (805-035-180) antibodies were from Jackson ImmunoResearch; secondary fluorophore-conjugated anti-rabbit IRDye 680 (926-68023) and anti-mouse IRDye 800CW (926-32212) antibodies used in the Odyssey system were from LICOR Biosciences. Secondary antibodies used for immunofluorescence: Alexa Fluor 488-, 555-, 647-conjugated anti-goat, anti-mouse and anti-rabbit were from ThermoFisher Scientific. All secondary antibodies were diluted 1:10,000.

For immunoprecipitation assay, goat agonistic anti-LTβR (AF629, R&D Systems) and control goat IgG (I5256, Sigma-Aldrich) were used.

Immunofluorescence staining and image analysis

Routinely, cells were transferred to ice, washed twice with ice-cold PBS, and fixed with ice-cold 3% paraformaldehyde for 15 min. After three washes with PBS, cells were processed directly for immunostaining, as described previously (Jastrzebski et al., 2017; Maminska et al., 2016; Sadowski et al., 2013).

To discriminate between LTβR exposed on the surface of endosomes from that sequestered inside ILVs, we used differential detergent solubilization as previously described (Malerod et al., 2007; Villasenor et al., 2016). Cells were fixed with 3.6% PFA for 7 min and permeabilized with 0.1% saponin (Sigma-Aldrich) for 10 min or with 0.001% digitonin (Abcam) for 1 min, washed twice with PBS and blocked for 30 min with 5 mg/ml BSA (Bioshop) and 0.2% gelatin from cold water fish skin (Sigma-Aldrich). Then cells were incubated for 1 h with mouse anti-LTβR, agonistic goat antibody against LTβR and rabbit anti-LAMP1. From this step, samples were processed as described previously (Jastrzebski et al., 2017; Maminska et al., 2016; Sadowski et al., 2013).

Slides were scanned using a ZEISS LSM 710 confocal microscope with EC Plan-Neofluar 40×1.3 NA oil immersion objective. ZEN 2009 software (Zeiss) was used for image acquisition. At least ten 12-bit images with resolution 1024×1024 pixels were acquired per experimental condition. Images were imported into MotionTracking (http://motiontracking.mpi-cbg.de) to analyze integral intensity or mean of integral intensity of fluorescence of LTβR in all vesicles (expressed in arbitrary units, AU) and the percentage of colocalization between two or three markers (Collinet et al., 2010; Kalaidzidis et al., 2015; Rink et al., 2005). Pictures were assembled in Photoshop (Adobe) with only linear adjustments of contrast and brightness.

Airyscan imaging and processing

Airyscan imaging was performed with a confocal laser scanning microscope ZEISS LSM 800 equipped with Plan-Apochromat 63×/1.40 NA oil objective and an Airyscan detection unit, using Immersol 518 F immersion media (Zeiss). Detector gain and pixel dwell times were adjusted for each dataset keeping them at their lowest values to avoid saturation and bleaching effects. ZEN Blue 2.3 (Version 2.3.69.1003) software (Zeiss) was used for image acquisition. The Airyscan processing module with default settings was used to process

obtained data. Pictures were assembled in Photoshop (Adobe) with only linear adjustments of contrast and brightness.

Transfection with small interfering RNA (siRNAs)

siRNA transfections were performed according to manufacturers' instructions using RNAiMAX (ThermoFisher Scientific) in HeLa cells or HiPerFect in HEK 293 cells (Qiagen). HeLa cells were seeded at a day of transfection on 12 mm coverslips in a 24-well plate (4 x 10^4 cells/well) for microscopic experiments, on a 12-well plate for qRT-PCR and Western blotting (7.5 x 10^4 cells/well) or on a 10 cm dish for immunoprecipitation experiments (1.1 x 10^6 cells/plate). HEK 293 cells were seeded one day before transfection in 6-well plates (8 x 10^5 cells/well) for microarray analysis. Cells were analyzed 72 h (HOPS-, CORVET- and Rab7-depleted cells) or 48 h (Vps28- and Tsg101-depleted cells) post transfection. For microarray analysis total RNA was isolated from HEK 293 cells 72 h after transfection. The concentration of siRNA in HeLa cells was 10 nM, except siRNAs targeting Tsg101 and Vps28 (2 nM) or Vps3 and Vps8 (20 nM). The concentration of siRNA in HEK 293 cells was 15 nM. The following Ambion Silencer Select siRNAs (ThermoFisher Scientific) were used: Ctrl_1 (Negative Control No. 1, 4390843), Ctrl_2 (Negative Control No. 2, 4390846), Rab7_1 (s15442), Rab7_2 (s15444), Tsg101_1 (s14440), Vps3_1 (s17973), Vps3_2 (s17974), Vps8_1 (s23635), Vps8_2 (s23637), Vps11_1 (s31595), Vps11_2 (s31597), Vps11_3 (s31596), Vps16_1 (s34802), Vps16_2 (s34803), Vps18_1 (s33451), Vps18_2 (s33453), Vps28_1 (s27579), Vps28_2 (s27577), Vps39_1 (s23601), Vps39_2 (s23599), Vps41_1 (s25768) and Vps41_2 (s25770).

Generation of Vps39 and Vps41 knockout HeLa cell lines by CRISPR/Cas9

Genome editing of HeLa cells was performed using a double-nicking strategy to knock out *VPS39* and *VPS41*. For each gene two 20-bp-long single guide RNA (sgRNAs) were designed based on Brunello library (Doench et al., 2016). To clone sgRNAs, BsmBI recognition sites were appended along with the appropriate overhang sequences to each pair of the oligonucleotides (Table S1), that then were annealed and ligated with gRNA expression LentiCRISPR v2 vector (Addgene vector #52961).

The sgRNA plasmids (4 μg) along with pPAX2 (3 μg) and pMD2.G (1 μg) were used for transfection of HEK 293T cells plated into 6-well plate (8 x 10^5 cells/well) to produce lentiviruses. 48 h post transfection Hela cells (plated one day before in 6-well format at 1.25 x 10^5 cells/well) were infected with the harvested viruses and grown for two days before

addition of puromycin (1.2 μg/ml). After ten days of selection for puromycin resistance, cells were plated in medium without antibiotic and analyzed.

Generation of Rab7 depletion in HeLa cells with shRNA

Small hairpin RNA (shRNA) targeting Rab7 (Primer sequence: Forward 5'-CCGGGTGTTGCTGAAGGTTATCACTGCAGTGATAACCTTCAGCAACACTTTTTG-3';

Reverse 5'-AATTCAAAAAGTGTTGCTGAAGGTTATCACTGCAGTGATAACCTTCAG CAACAC-3') was cloned into lentiviral vector pLKO.1 TRC cloning vector (Addgene #10878). Lentiviral vectors pLKO.1 - TRC control (Addgene #10879) and scramble shRNA (Addgene #1864) were used as controls. The shRNA plasmids (4 μg) along with pPAX2 (3 μg) and pMD2.G (1 μg) were used for transfection of HEK 293T cells plated into 6-well plate (8 x 10^5 cells/well) to produce lentiviruses. 48 h post transfection Hela cells (plated one day before in 6-well format at 1 x 10^5 cells/well) were infected with the harvested viruses and grown for two days before selection for puromycin resistance (1 μg/ml). After seven days of selection cells were plated in medium without antibiotic and analyzed.

Rab7 rescue experiement

HeLa cells (4 x 10^4 cells/well in 24-well format) were transfected with 10 nM siRNA against Rab7 or control siRNA. After 24 h cells were transfected with 0.5 μg of plasmid encoding canine Rab7 protein (pcDNA3 HA-Rab7, gift from Prof. Cecilia Bucci) or control pcDNA3-HA-NI (gift from Prof. Kazuhisa Nakayama) using FuGENE 6 (Promega) according to manufacturer's instructions. The nucleotide sequence of dog Rab7 construct is resistant to silencing with Rab7_2 siRNA (two nucleotide mismatches) but not Rab7_1 siRNA (complete match). After 72 h (starting from the transfection with siRNA) cells were fixed with paraformaldehyde and analyzed by immunofluorescence staining as described above.

Western blotting

Hela cells were lysed in RIPA buffer (1% Triton X-100, 0.5% sodium deoxycholate, 0.1% SDS, 50 mM Tris pH 7.4, 150 mM NaCl, 0.5 mM EDTA) supplemented with protease inhibitor cocktail (6 μg/ml chymostatin, 0.5 μg/ml leupeptin, 10 μg/ml antipain, 2 μg/ml aprotinin, 0.7 μg/ml pepstatin A and 10 μg/ml 4-amidinophenylmethanesulfonyl fluoride hydrochloride; Sigma-Aldrich) and phosphatase inhibitor cocktails (Sigma-Aldrich, P0044 and P5726). Protein concentration was measured with BCA Protein Assay Kit (ThermoFisher

Scientific). 10-50 µg of total protein per sample were resolved on SDS-PAGE, transferred to nitrocellulose membrane (Whatman), probed with specific primary and secondary antibodies, and detected using ChemiDoc imaging system (Bio-Rad) or Odyssey infrared imaging system (LI-COR Biosciences). Densitometry of protein bands was carried out using ImageJ Software (Schneider et al., 2012).

Immunoprecipitation (IP)

HeLa cell lysates were prepared in RIPA buffer. 250-500 µg of protein was used per reaction. Cell extracts were diluted in immunoprecipitation (IP) buffer (50 mM HEPES, pH 7.5, 150 mM NaCl, 1 mM EGTA, 1 mM EDTA, 1% Triton X-100, 10% glycerol, 5 µg/ml DNase and protease inhibitor cocktail) and pre-cleared for 3 h at 4°C with goat IgG (Sigma-Aldrich) and Protein G agarose beads (Roche) to deplete nonspecifically bound proteins. Pre-cleared cell lysates were incubated overnight at 4°C with 2.5 µg of antibodies (specific anti-LTβR or unspecific goat IgG) with constant rotation. Immune complexes were recovered by 2 h incubation with Protein G–agarose beads at 4°C with rotation. The agarose beads with bound protein complexes were spun down and washed four times using IP buffer. Next, samples were incubated at 95°C for 10 min with Laemmli buffer and subjected to electrophoresis on 10% polyacrylamide gels.

Quantitative real-time PCR (qRT-PCR)

Total RNA was isolated with High Pure Isolation Kit (Roche). For cDNA synthesis random nonamers, oligo(dT)23 and M-MLV reverse transcriptase (Sigma-Aldrich) were used according to manufacturer's instructions. To estimate the expression of genes of interest we used primers designed with NCBI tool (and custom-synthesized by Sigma-Aldrich) listed in Table S2 or TaqMan® Gene Expression Assays (ThermoFisher Scientific) listed in Table S3.

The qRT-PCR reaction was performed with the KAPA SYBR FAST qPCR Master Mix (2X) Universal Kit (KK4618, KapaBiosystems) or TaqMan® Gene Expression Master Mix (4369016, ThermoFisher Scientific) using a 7900HT Fast Real-Time PCR thermocycler (Applied Biosystems) with at least two technical repeats per experimental condition. The data were normalized according to the level of housekeeping genes *ACTB*, *B2M,* and *GAPDH* and presented as fold changes.

Microarray analysis

HEK 293 cells were transfected with control (Ctrl_1 or Ctrl_2) or HOPS-targeting (Vps11_1, Vps39_1, Vps39_2, Vps41_1 or Vps41_2) siRNAs in three biological repetitions (21 samples in total). A starting amount of 200 ng of high-quality total RNA was used to generate cDNA and cRNA with the Illumina TotalPrep RNA Amplification Kit (Illumina). The cRNA samples were prepared according to a procedure described elsewhere (Pera et al., 2013). Each cRNA sample (1.5 μg) was hybridized overnight using the Human HT-12 BeadChip array (Illumina) in a multiple-step procedure; the chips were washed, dried, and scanned on the BeadArray Reader (Illumina). Raw microarray data were generated using BeadStudio v3.0 (Illumina). A total of 21 Illumina HumanHT-12v4 microarrays were used in the experiment. To provide an appropriate balance in the entire data set, the groups were equally divided between the array plates and the hybridization batches. Microarray analysis and quality control of the arrays were performed using BeadArray R package v1.10.0. After background subtraction (using median background method), the data were normalized using quantile normalization and were subsequently log2-transformed. The obtained signal was taken as the measure of mRNA abundance derived from the level of gene (or its particular transcriptional variant) expression.

Statistical analysis of the results was performed using a t-test followed by correction for multiple testing using false discovery rate (FDR). The false discovery rate was estimated using the Benjamini and Hochberg method. All statistical analyses were performed using R software (https://www.r-project.org/).

Differentially expressed genes were investigated for putative cellular functions. Over-represented functional groups of genes were obtained from gene ontology (GO) DAVID 6.7 database at http://david.abcc.ncifcrf.gov (Huang da et al., 2009).

Statistical analysis

At least 3 independent experiments were performed in each case. Statistical testing was performed using Prism 6 (GraphPad Software). Data were analyzed for Gaussian distribution with a Kolmogorov-Smirnov test with the Dallal-Wilkinson-Lilliefor corrected P value. In case of Gaussian distribution, the following parametric tests were used: Student's t-test or one-way ANOVA with Dunnett's post-hoc test, as appropriate. In case of non-Gaussian distribution, the following nonparametric tests were used: Mann-Whitney or Kruskal-Wallis

with Dunn's post-hoc test. The significance of mean comparison is annotated as follows: ns, non-significant (P>0.05), *P≤0.05, **P≤0.01, and ***P≤0.001. No statistical methods were used to predetermine sample size.

Author contributions

MBO designed, performed and analyzed experiments in Fig. 2E-F; 3E; 4; 5E-F; S2; S3C, S4A, D; S5A and wrote the manuscript; KJ designed, performed and analyzed experiments in Fig. 1A-D; 2A-D; 3A-D, F-G; 5A-D, 6A-C, S1A,B,D; S2, S3A,B, S6 and wrote the manuscript; JC designed, performed and analyzed experiments in Fig. S5C-E; MMaksymowicz contributed data to Fig. 2F; 4B, C; 5A-D; S2E and performed experiments in S4B,C; KW contributed data to Fig. 1E; Fig. 5A-D; S1C; S2E,F; MK performed the microarray analysis; DM and JG contributed to design and analysis of experiments; MMiaczynska conceived, designed and analyzed experiments and wrote the manuscript.

References

Balderhaar, H. J., Lachmann, J., Yavavli, E., Brocker, C., Lurick, A. and Ungermann, C. (2013). The CORVET complex promotes tethering and fusion of Rab5/Vps21-positive membranes. *Proc Natl Acad Sci U S A* **110**, 3823-8.

Balderhaar, H. J. and Ungermann, C. (2013). CORVET and HOPS tethering complexes - coordinators of endosome and lysosome fusion. *J Cell Sci* **126**, 1307-16.

Barbieri, E., Di Fiore, P. P. and Sigismund, S. (2016). Endocytic control of signaling at the plasma membrane. *Curr Opin Cell Biol* **39**, 21-7.

Brankatschk, B., Wichert, S. P., Johnson, S. D., Schaad, O., Rossner, M. J. and Gruenberg, J. (2012). Regulation of the EGF transcriptional response by endocytic sorting. *Sci Signal* **5**, ra21.

Cendrowski, J., Maminska, A. and Miaczynska, M. (2016). Endocytic regulation of cytokine receptor signaling. *Cytokine Growth Factor Rev* **32**, 63-73.

Chang, Y. H., Hsieh, S. L., Chen, M. C. and Lin, W. W. (2002). Lymphotoxin beta receptor induces interleukin 8 gene expression via NF-kappaB and AP-1 activation. *Exp Cell Res* **278**, 166-74.

Christ, L., Raiborg, C., Wenzel, E. M., Campsteijn, C. and Stenmark, H. (2017). Cellular Functions and Molecular Mechanisms of the ESCRT Membrane-Scission Machinery. *Trends Biochem Sci* **42**, 42-56.

Collinet, C., Stoter, M., Bradshaw, C. R., Samusik, N., Rink, J. C., Kenski, D., Habermann, B., Buchholz, F., Henschel, R., Mueller, M. S. et al. (2010). Systems survey of endocytosis by multiparametric image analysis. *Nature* **464**, 243-9.

Dejardin, E., Droin, N. M., Delhase, M., Haas, E., Cao, Y., Makris, C., Li, Z. W., Karin, M., Ware, C. F. and Green, D. R. (2002). The lymphotoxin-beta receptor induces different patterns of gene expression via two NF-kappaB pathways. *Immunity* **17**, 525-35.

Dobrowolski, R., Vick, P., Ploper, D., Gumper, I., Snitkin, H., Sabatini, D. D. and De Robertis, E. M. (2012). Presenilin deficiency or lysosomal inhibition enhances Wnt signaling through relocalization of GSK3 to the late-endosomal compartment. *Cell Rep* **2**, 1316-28.

Doench, J. G., Fusi, N., Sullender, M., Hegde, M., Vaimberg, E. W., Donovan, K. F., Smith, I., Tothova, Z., Wilen, C., Orchard, R. et al. (2016). Optimized sgRNA design to maximize activity and minimize off-target effects of CRISPR-Cas9. *Nat Biotechnol* **34**, 184-191.

Frankel, E. B. and Audhya, A. (2018). ESCRT-dependent cargo sorting at multivesicular endosomes. *Semin Cell Dev Biol* **74**, 4-10.

Ganeff, C., Remouchamps, C., Boutaffala, L., Benezech, C., Galopin, G., Vandepaer, S., Bouillenne, F., Ormenese, S., Chariot, A., Schneider, P. et al. (2011). Induction of the alternative NF-kappaB pathway by lymphotoxin alphabeta (LTalphabeta) relies on internalization of LTbeta receptor. *Mol Cell Biol* **31**, 4319-34.

Guerra, F. and Bucci, C. (2016). Multiple Roles of the Small GTPase Rab7. *Cells* **5**.

Huang da, W., Sherman, B. T. and Lempicki, R. A. (2009). Systematic and integrative analysis of large gene lists using DAVID bioinformatics resources. *Nat Protoc* **4**, 44-57.

Huotari, J. and Helenius, A. (2011). Endosome maturation. *EMBO J* **30**, 3481-500.

Jastrzebski, K., Zdzalik-Bielecka, D., Maminska, A., Kalaidzidis, Y., Hellberg, C. and Miaczynska, M. (2017). Multiple routes of endocytic internalization of PDGFRbeta contribute to PDGF-induced STAT3 signaling. *J Cell Sci* **130**, 577-589.

Jonker, C. T. H., Galmes, R., Veenendaal, T., Ten Brink, C., van der Welle, R. E. N., Liv, N., de Rooij, J., Peden, A. A., van der Sluijs, P., Margadant, C. et al. (2018). Vps3 and Vps8 control integrin trafficking from early to recycling endosomes and regulate integrin-dependent functions. *Nat Commun* **9**, 792.

Kalaidzidis, Y., Kalaidzidis, I. and Zerial, M. (2015). A Probabilistic Method to Quantify the Colocalization of Markers on Intracellular Vesicular Structures Visualized by Light Microscopy. *Bayesian Inference and Maximum Entropy Methods in Science and Engineering (Maxent 2014)* **1641**, 580-587.

Khatter, D., Raina, V. B., Dwivedi, D., Sindhwani, A., Bahl, S. and Sharma, M. (2015). The small GTPase Arl8b regulates assembly of the mammalian HOPS complex on lysosomes. *J Cell Sci* **128**, 1746-61.

Kim, Y. S., Nedospasov, S. A. and Liu, Z. G. (2005). TRAF2 plays a key, nonredundant role in LIGHT-lymphotoxin beta receptor signaling. *Mol Cell Biol* **25**, 2130-7.

Lin, X., Yang, T., Wang, S., Wang, Z., Yun, Y., Sun, L., Zhou, Y., Xu, X., Akazawa, C., Hong, W. et al. (2014). RILP interacts with HOPS complex via VPS41 subunit to regulate endocytic trafficking. *Sci Rep* **4**, 7282.

Malerod, L., Stuffers, S., Brech, A. and Stenmark, H. (2007). Vps22/EAP30 in ESCRT-II mediates endosomal sorting of growth factor and chemokine receptors destined for lysosomal degradation. *Traffic* **8**, 1617-29.

Maminska, A., Bartosik, A., Banach-Orlowska, M., Pilecka, I., Jastrzebski, K., Zdzalik-Bielecka, D., Castanon, I., Poulain, M., Neyen, C., Wolinska-Niziol, L. et al. (2016). ESCRT proteins restrict constitutive NF-kappaB signaling by trafficking cytokine receptors. *Sci Signal* **9**, ra8.

Markgraf, D. F., Ahnert, F., Arlt, H., Mari, M., Peplowska, K., Epp, N., Griffith, J., Reggiori, F. and Ungermann, C. (2009). The CORVET subunit Vps8 cooperates with the Rab5 homolog Vps21 to induce clustering of late endosomal compartments. *Mol Biol Cell* **20**, 5276-89.

Miaczynska, M. (2013). Effects of membrane trafficking on signaling by receptor tyrosine kinases. *Cold Spring Harb Perspect Biol* **5**, a009035.

Muller, J. R. and Siebenlist, U. (2003). Lymphotoxin beta receptor induces sequential activation of distinct NF-kappa B factors via separate signaling pathways. *J Biol Chem* **278**, 12006-12.

Nakano, H., Oshima, H., Chung, W., Williams-Abbott, L., Ware, C. F., Yagita, H. and Okumura, K. (1996). TRAF5, an activator of NF-kappaB and putative signal transducer for the lymphotoxin-beta receptor. *J Biol Chem* **271**, 14661-4.

Peplowska, K., Markgraf, D. F., Ostrowicz, C. W., Bange, G. and Ungermann, C. (2007). The CORVET tethering complex interacts with the yeast Rab5 homolog Vps21 and is involved in endo-lysosomal biogenesis. *Dev Cell* **12**, 739-50.

Pera, J., Korostynski, M., Golda, S., Piechota, M., Dzbek, J., Krzyszkowski, T., Dziedzic, T., Moskala, M., Przewlocki, R., Szczudlik, A. et al. (2013). Gene expression profiling of blood in ruptured intracranial aneurysms: in search of biomarkers. *J Cereb Blood Flow Metab* **33**, 1025-31.

Perini, E. D., Schaefer, R., Stoter, M., Kalaidzidis, Y. and Zerial, M. (2014). Mammalian CORVET is required for fusion and conversion of distinct early endosome subpopulations. *Traffic* **15**, 1366-89.

Poteryaev, D., Datta, S., Ackema, K., Zerial, M. and Spang, A. (2010). Identification of the switch in early-to-late endosome transition. *Cell* **141**, 497-508.

Price, A., Seals, D., Wickner, W. and Ungermann, C. (2000). The docking stage of yeast vacuole fusion requires the transfer of proteins from a cis-SNARE complex to a Rab/Ypt protein. *J Cell Biol* **148**, 1231-8.

Remouchamps, C., Boutaffala, L., Ganeff, C. and Dejardin, E. (2011). Biology and signal transduction pathways of the Lymphotoxin-alphabeta/LTbetaR system. *Cytokine Growth Factor Rev* **22**, 301-10.

Rink, J., Ghigo, E., Kalaidzidis, Y. and Zerial, M. (2005). Rab conversion as a mechanism of progression from early to late endosomes. *Cell* **122**, 735-49.

Sadowski, L., Jastrzebski, K., Kalaidzidis, Y., Heldin, C. H., Hellberg, C. and Miaczynska, M. (2013). Dynamin inhibitors impair endocytosis and mitogenic signaling of PDGF. *Traffic* **14**, 725-36.

Schneider, C. A., Rasband, W. S. and Eliceiri, K. W. (2012). NIH Image to ImageJ: 25 years of image analysis. *Nat Methods* **9**, 671-5.

Scott, C. C., Vacca, F. and Gruenberg, J. (2014). Endosome maturation, transport and functions. *Semin Cell Dev Biol* **31**, 2-10.

Spang, A. (2016). Membrane Tethering Complexes in the Endosomal System. *Front Cell Dev Biol* **4**, 35.

Szymanska, E., Budick-Harmelin, N. and Miaczynska, M. (2018). Endosomal "sort" of signaling control: The role of ESCRT machinery in regulation of receptor-mediated signaling pathways. *Semin Cell Dev Biol* **74**, 11-20.

Taelman, V. F., Dobrowolski, R., Plouhinec, J. L., Fuentealba, L. C., Vorwald, P. P., Gumper, I., Sabatini, D. D. and De Robertis, E. M. (2010). Wnt signaling requires sequestration of glycogen synthase kinase 3 inside multivesicular endosomes. *Cell* **143**, 1136-48.

VanArsdale, T. L., VanArsdale, S. L., Force, W. R., Walter, B. N., Mosialos, G., Kieff, E., Reed, J. C. and Ware, C. F. (1997). Lymphotoxin-beta receptor signaling complex: role of tumor necrosis factor receptor-associated factor 3 recruitment in cell death and activation of nuclear factor kappaB. *Proc Natl Acad Sci U S A* **94**, 2460-5.

Varfolomeev, E., Goncharov, T., Maecker, H., Zobel, K., Komuves, L. G., Deshayes, K. and Vucic, D. (2012). Cellular inhibitors of apoptosis are global regulators of NF-kappaB and MAPK activation by members of the TNF family of receptors. *Sci Signal* **5**, ra22.

Villasenor, R., Kalaidzidis, Y. and Zerial, M. (2016). Signal processing by the endosomal system. *Curr Opin Cell Biol* **39**, 53-60.

Vince, J. E., Chau, D., Callus, B., Wong, W. W., Hawkins, C. J., Schneider, P., McKinlay, M., Benetatos, C. A., Condon, S. M., Chunduru, S. K. et al. (2008). TWEAK-FN14 signaling induces lysosomal degradation of a cIAP1-TRAF2 complex to sensitize tumor cells to TNFalpha. *J Cell Biol* **182**, 171-84.

Zhang, Q., Lenardo, M. J. and Baltimore, D. (2017). 30 Years of NF-kappaB: A Blossoming of Relevance to Human Pathobiology. *Cell* **168**, 37-57.

Figures
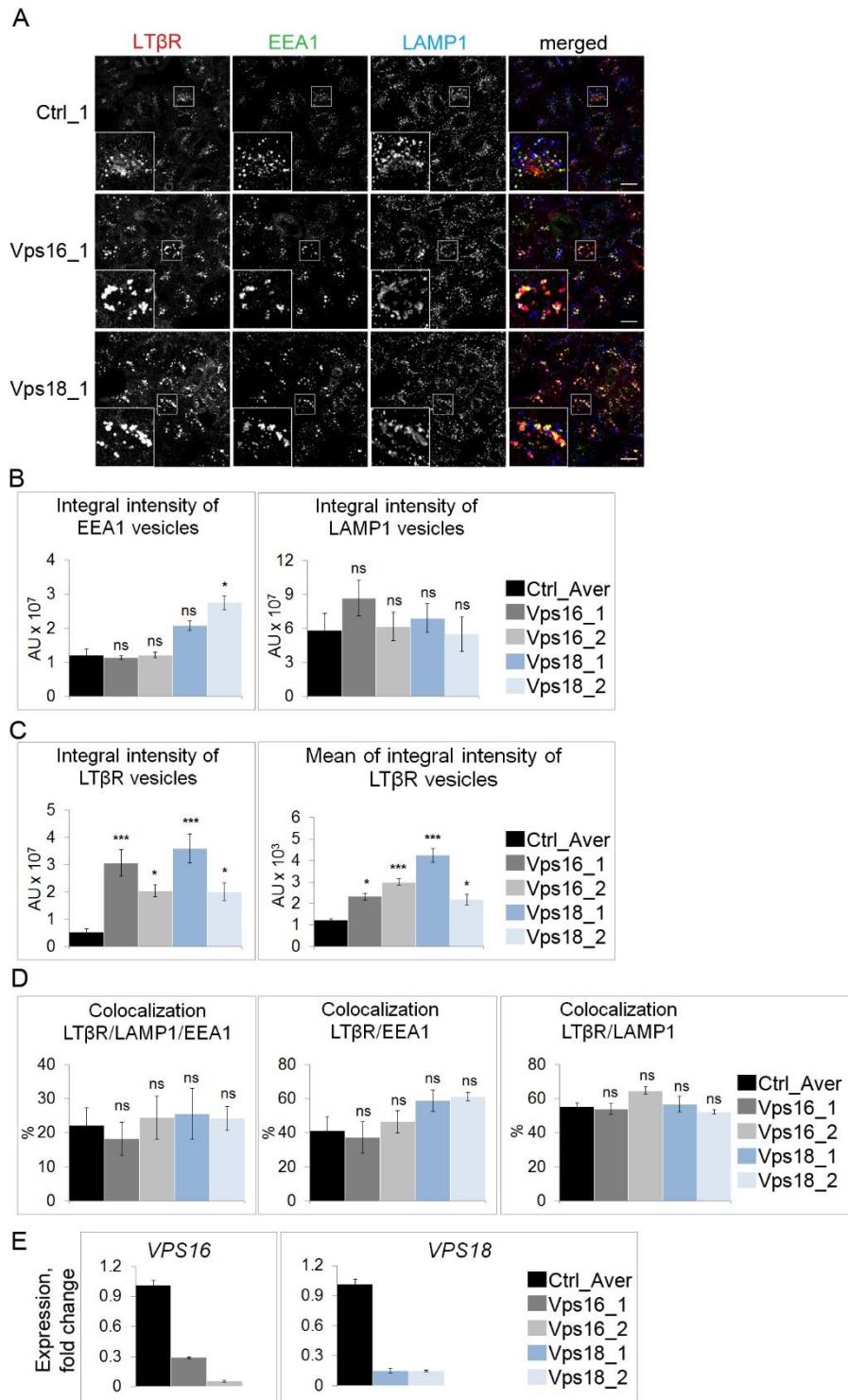
Figure 1. Depletion of common HOPS/CORVET components affects intracellular distribution of LTβR.

A   Immunofluorescence staining of LTβR, EEA1 and LAMP1 in HeLa cells upon knockdown of Vps16 or Vps18 and in control (Ctrl) siRNA-transfected cells. Insets: Magnified views of boxed regions in the main images. Scale bars, 20 µm.

B   Analysis of integral intensities of EEA1- and LAMP1-positive vesicles in cells depleted of Vps16 or Vps18 (two independent siRNA oligonucleotides per gene).

C   Analysis of integral and mean of integral intensities of LTβR-positive vesicles in cells depleted of Vps16 or Vps18 (as above).

D   Analysis of colocalization between LTβR, LAMP1 and EEA1; LTβR and EEA1; LTβR and LAMP1 in cells depleted of Vps16 or Vps18 (as above).

E   qRT-PCR analysis of the silencing efficiency of *VPS16* or *VPS18* in HeLa cells.

Data information: Black bars (Ctrl_Aver) in B-E represent values averaged of two non-targeting siRNAs transfected independently (Ctrl_1 and Ctrl_2). Data represent the means ± SEM, n=4 (B); n≥3 (C); n=4 (D); n=3 (E). ns - $P > 0.05$; *$P \leq 0.05$; ***$P \leq 0.001$ in B, C and D by ANOVA or Kruskal-Wallis test.
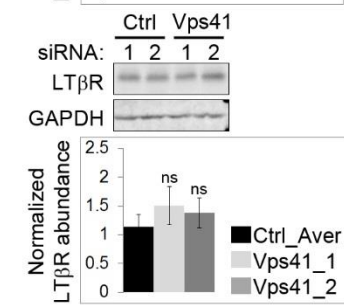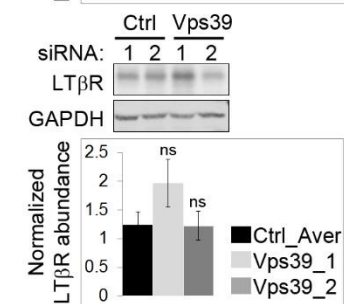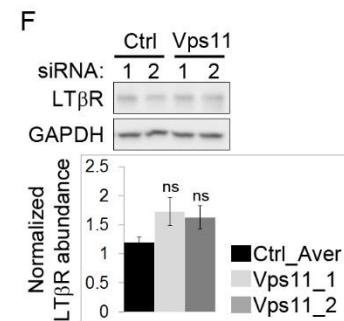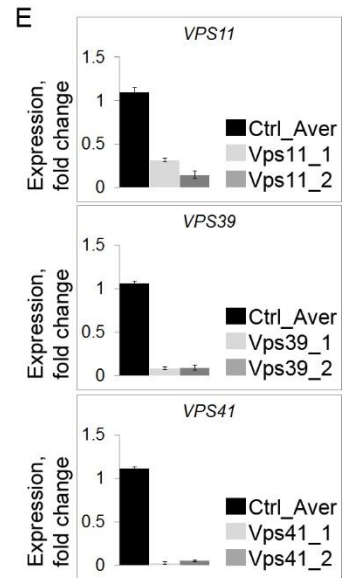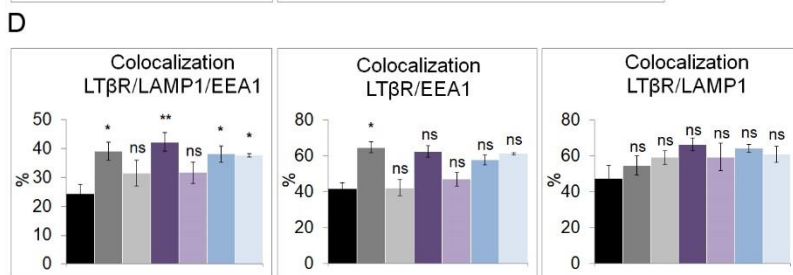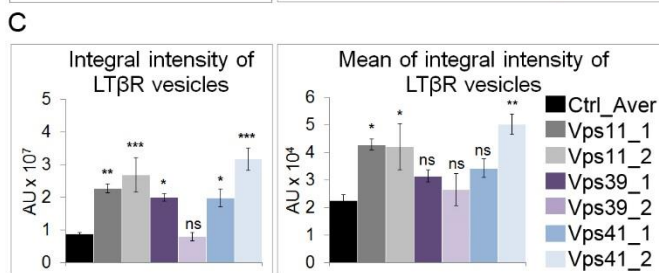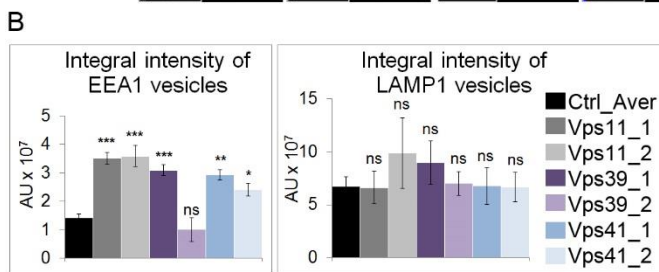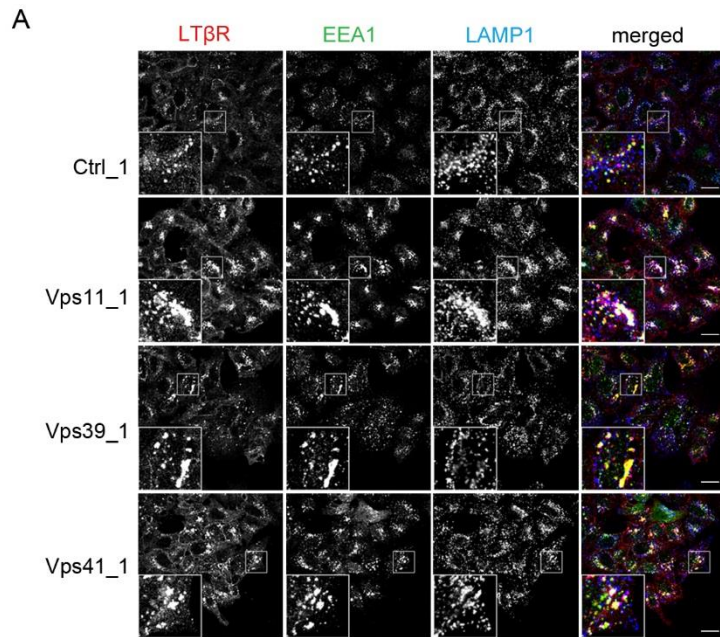
Figure 2. Depletion of HOPS complex leads to endosomal accumulation of LTβR.

A   Immunofluorescence staining of LTβR, EEA1, and LAMP1 in HeLa cells upon knockdown of the indicated HOPS components or in control (Ctrl) siRNA-transfected cells. Insets: Magnified views of boxed regions in the main images. Scale bars, 20 µm.

B   Analysis of integral intensities of EEA1- and LAMP1-positive vesicles in cells with HOPS knockdown (two independent siRNA oligonucleotides per gene).

C   Analysis of integral and mean of integral intensities of LTβR-positive vesicles in cells with HOPS knockdown (as above).

D   Analysis of colocalization between LTβR, LAMP1 and EEA1; LTβR and EEA1; LTβR and LAMP1 in cells depleted of the indicated HOPS components. The color-code as in B and C.

E   qRT-PCR analysis of the silencing efficiency of *VPS11, VPS39* or *VPS41* in HeLa cells.

F   Lysates of HeLa cells depleted of the indicated HOPS subunits were analyzed by Western blotting with antibodies against LTβR, with GAPDH used as a loading control. Graphs depict quantification of LTβR abundance.

Data information: Black bars (Ctrl_Aver) in B-F represent values averaged of two non-targeting siRNAs transfected independently (Ctrl_1 and Ctrl_2). Data represent the means ± SEM, n=4 (B); n=4 (C); n=3 (D); n=3(E); n≥3 (F). Statistical significance was evaluated (in B-D and F) using ANOVA test or Kruskal-Wallis test. ns - P>0.05; *P≤0.05; **P≤0.01; ***P≤0.001.
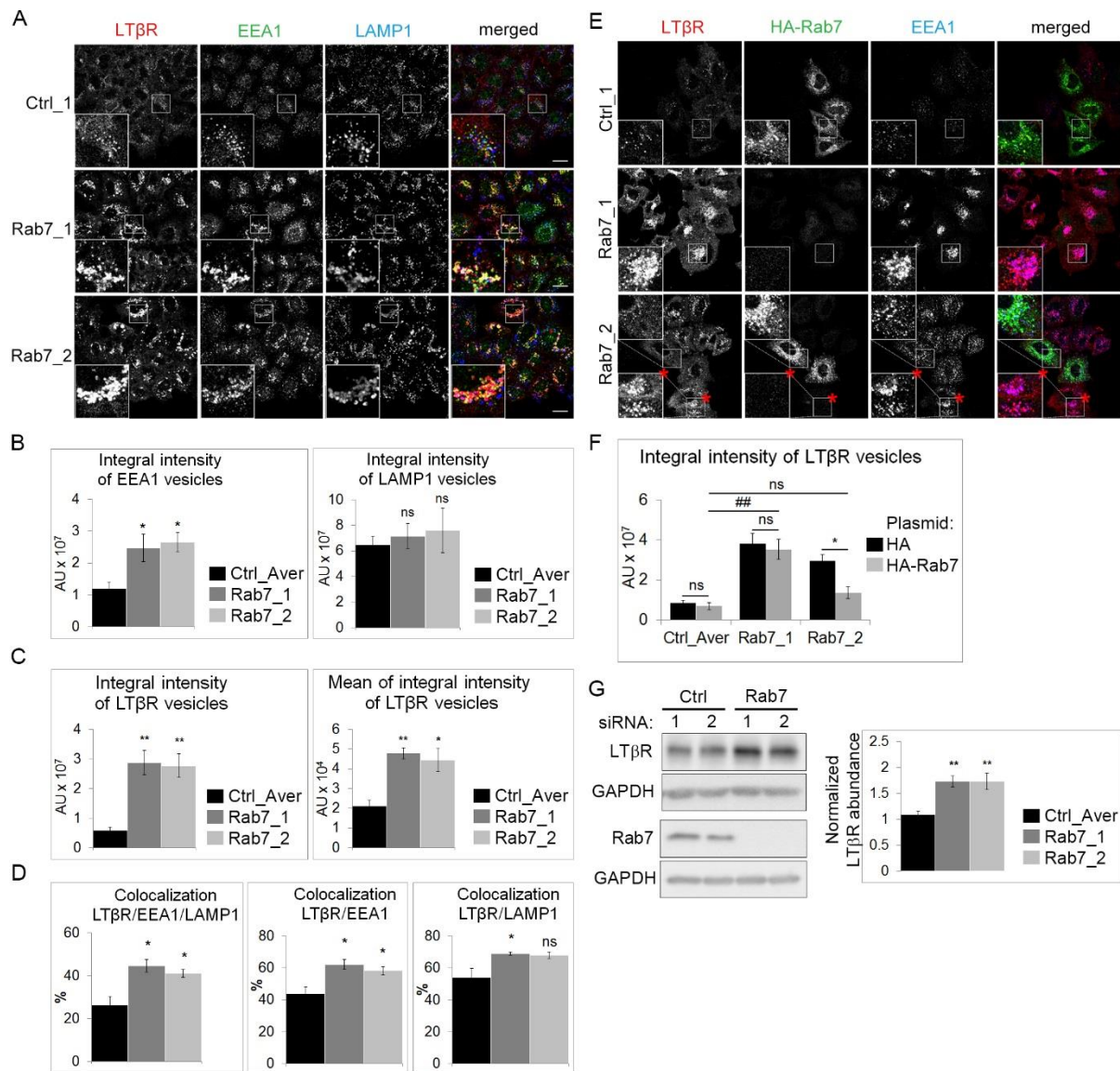
Figure 3. Depletion of Rab7 causes endosomal accumulation of LTβR and increases the total level of the receptor.

A   Immunofluorescence staining of LTβR, EEA1 and LAMP1 in HeLa cells upon knockdown of Rab7 or in control (Ctrl) siRNA-transfected cells. Insets: Magnified views of boxed regions in the main images. Scale bars, 20 µm.

B   Analysis of integral intensities of EEA1- and LAMP1-positive vesicles in cells depleted of Rab7 with two independent siRNA oligonucleotides.

C   Analysis of integral and mean of integral intensities of LTβR-positive vesicles in cells depleted of Rab7 (as above).

D   Analysis of colocalization between LTβR, LAMP1 and EEA1; LTβR and EEA1; LTβR and LAMP1 in cells depleted of Rab7 (as above; color-code as in B and C).

E   Immunofluorescence staining of LTβR, HA-tagged Rab7 and EEA1 in HeLa cells transfected with Rab7-targeting or control non-targeting (Ctrl) siRNAs, and the plasmid encoding HA-Rab7 fusion protein resistant to Rab7_2 siRNA but sensitive to Rab7_1 siRNA. Insets: Magnified views of boxed regions in the main images. Scale bars, 20 µm. The asterisk marks cells not transfected with HA-Rab7.

F   Analysis of integral intensity of LTβR-positive vesicles in HeLa cells transfected with Rab7-targeting or control non-targeting (Ctrl) siRNAs (two independent oligonucleotides in each case), and the plasmid encoding HA-Rab7 fusion or control plasmid encoding HA-tag.

G   Lysates of HeLa cells depleted of Rab7 were analyzed by Western blotting with antibodies against LTβR or Rab7, with GAPDH used as a loading control. Graph depicts quantification of LTβR abundance upon Rab7 knockdown.

Data information: Black bars (Ctrl_Aver) in B-D and G represent values averaged of two non-targeting siRNAs transfected independently (Ctrl_1 and Ctrl_2). Data represent the means ± SEM, n=4 (B); n=3 (C); n=3 (D); n=3 (F); n=4 (G). ns - P>0.05; *P≤0.05; **P≤0.01; [##] P≤0.01 by ANOVA or Student's t-test.
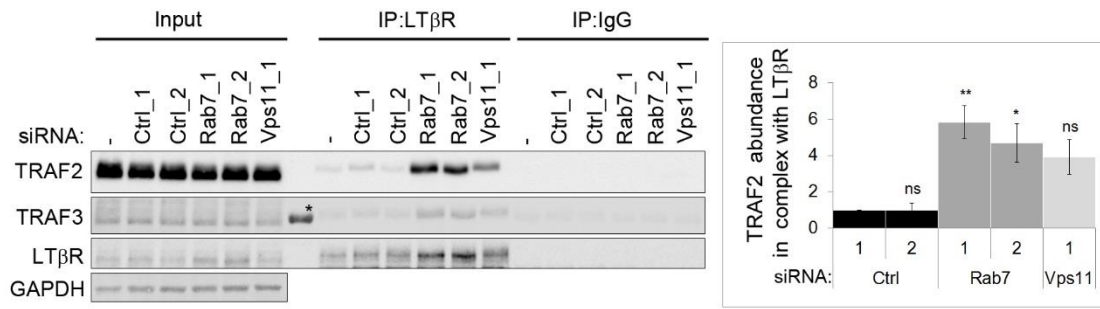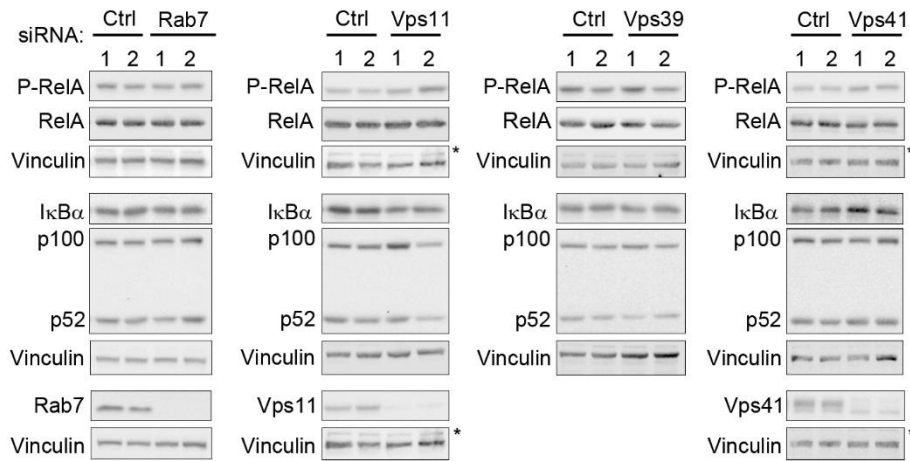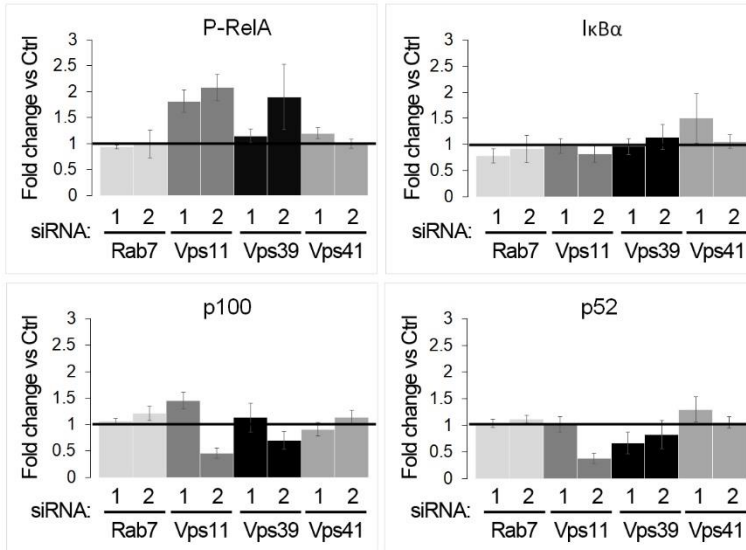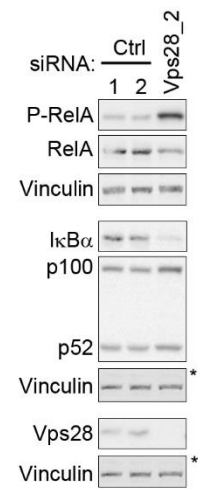
Figure 4. Rab7- and Vps11-depleted cells show increased LTβR-TRAF association that does not activate the NF-κB pathway.

A   (Left panel) Western blot analysis of immunoprecipitation (IP) of LTβR in extracts of HeLa cells transfected with non-targeting (Ctrl) or Rab7- and Vps11-targeting siRNA. Antibodies against LTβR, TRAF2 and TRAF3 were used for blotting, with GAPDH as a loading control. Input represents 10% of lysates used for IP. An asterisk marks an unspecific band of the molecular weight marker. (Right panel) TRAF2 abundance in LTβR immunoprecipitates upon knockdown of Rab7 and Vps11 was quantified as a ratio of co-immunoprecipitated TRAF2 to immunoprecipitated LTβR. Data were normalized to the TRAF2-LTβR ratio in Ctrl_1 siRNA-transfected cells, which was assigned a value of 1. Data represent the means ± SEM, n=3. ns - P>0.05; *P≤0.05; **P≤0.01 by ANOVA test.

B, D   Lysates of HeLa cells depleted of Rab7 and HOPS subunits (B) or ESCRT-I subunit Vps28 (D) were analyzed by Western blotting with antibodies against the indicated markers of NF-κB activation and the depleted proteins, with vinculin as a loading control. Blots are representative of three experiments. Asterisks indicate the same blots of vinculin within each panel, presented twice for clarity. Knockdown efficiency of Vps39 was tested by qRT-PCR as shown in Fig. 2E, as no available antibody worked on Western blots.

C   Abundance of P-RelA, IκBα, p100 and p52 proteins in extracts of Hela cells transfected with siRNAs targeting Rab7 and HOPS subunits was analyzed by Western botting (representative blots shown in B), quantified and presented as a fold change versus Ctrl_ Aver (averaged Ctrl_1 and Ctrl_2), which was assigned a value of 1. Data represent the means ± SEM, n≥3, except Vps41_1 (n=2).
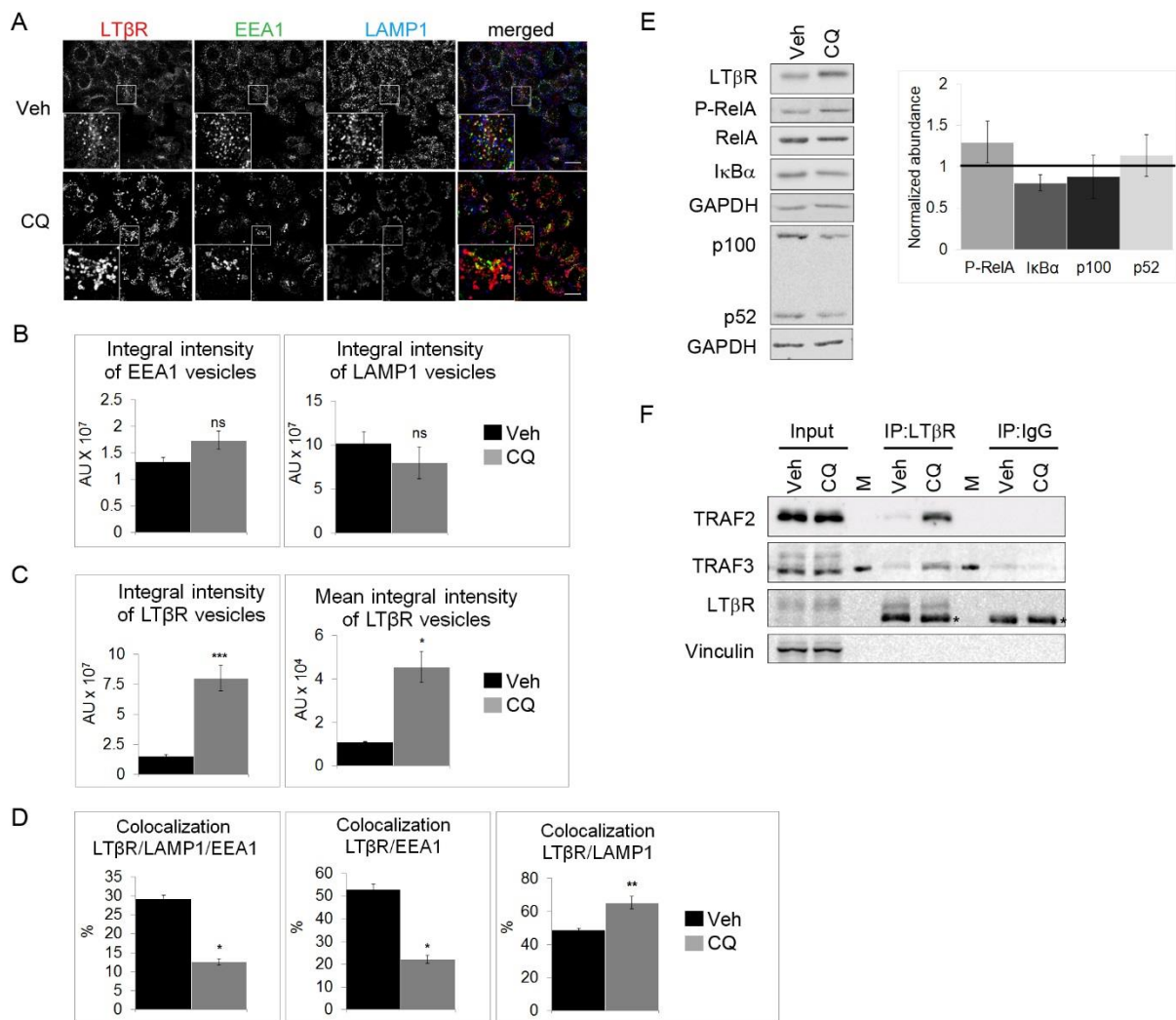
Figure 5. Inhibition of lysosomal degradation leads to endosomal accumulation of LTβR and its increased binding to TRAF proteins without activating the NF-κB pathway.

A   Immunofluorescence staining of LTβR, EEA1 and LAMP1 in HeLa cells treated with lysosomal inhibitor chloroquine (CQ) or vehicle (Veh). Insets: Magnified views of boxed regions in the main images. Scale bars, 20 µm.

B, C, D   Analysis of integral intensities of EEA1- and LAMP1-positive vesicles (B), integral and mean of integral intensities of LTβR-positive vesicles (C), colocalization between LTβR, LAMP1 and EEA1; LTβR and EEA1; LTβR and LAMP1 (D) in cells treated with chloroquine (CQ) or vehicle (Veh).

Data information: (B-D) Data represent the means ± SEM, n=4. *P≤0.05; **P≤0.01; ***P≤0.001 by Student's t-test.

E   Lysates of HeLa cells treated with chloroquine (CQ) or vehicle (Veh) were analyzed by Western blotting with antibodies against the indicated markers of NF-κB activation, with GAPDH as a loading control. Blots are representative of three experiments. (Right graph) Abundance of P-RelA, IκBα, p100 and p52 proteins in Hela cells treated with chloroquine (CQ) was quantified and presented as a fold change versus control (Veh), which was assigned a value of 1. Data represent the means ± SEM, n=3.

F   Western blot analysis of immunoprecipitation (IP) of LTβR from extracts of HeLa cells treated with CQ or vehicle. Antibodies against LTβR, TRAF2 and TRAF3 were used for blotting, with vinculin as a loading control. Input represents 10% of lysates used for IP. Asterisks mark heavy chain of antibodies used for IP. Blots are representative of two experiments. M – lane loaded with molecular weight marker.

A

	LTβR	EEA1	merged
Ctrl_1			
Tsg101_1			
Vps28_1			
Vps11_1			
Vps39_1			
Vps41_1			
Rab7_1			

B

Veh			
CQ			

C

Fraction of LTβR signal on the outer membrane of endosomes

- Tsg101_1
- Vps28_1
- Vps11_1
- Vps39_1
- Vps41_1
- Vps41_2
- Rab7_1
- Rab7_2

***

D

LTβR, Plasma membrane, ESCRT, NF-κB signaling, LTβR accumulation on the limiting membrane, HOPS Rab7, NF-κB signaling, LTβR sequestration in ILVs
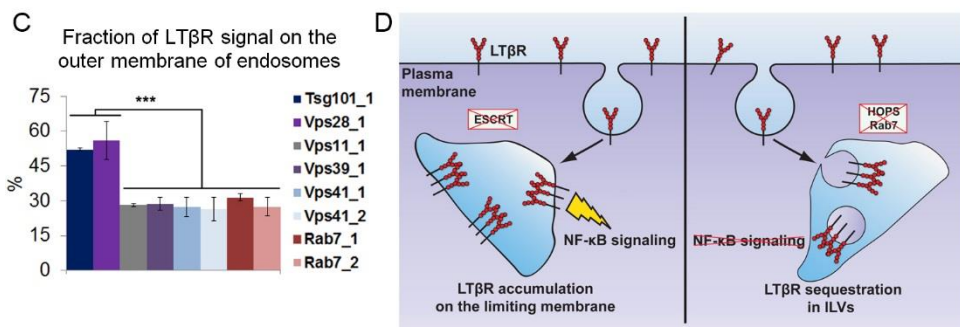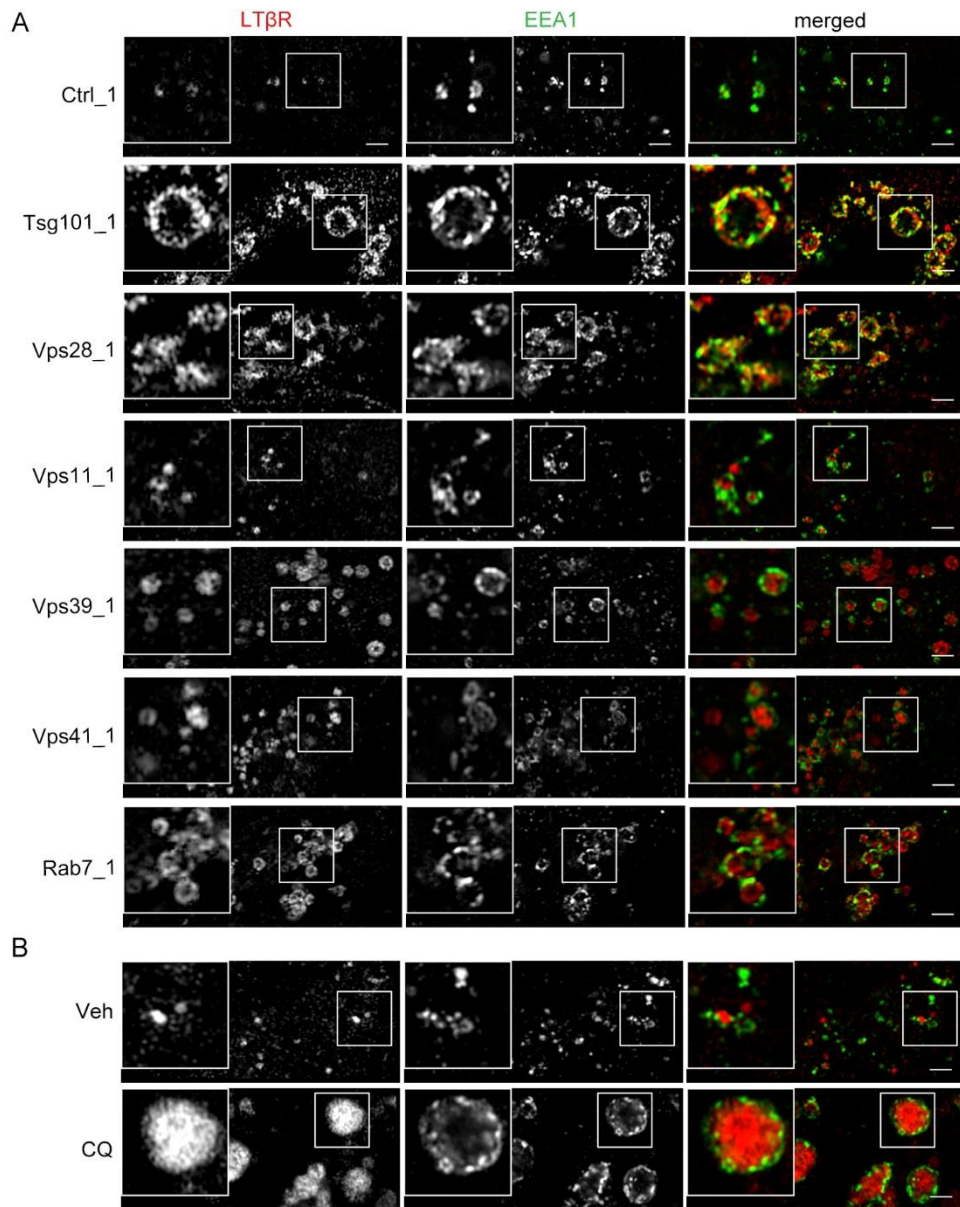
Figure 6. The topology of LTβR accumulated on EEA1-positive endosomes in cells depleted of HOPS or defective in lysosomal degradation is different than in ESCRT-I-depleted cells.

A, B   High-resolution images of HeLa cells transfected with siRNAs targeting the indicated ESCRT-I subunits (Tsg101, Vps28), HOPS components, Rab7 or with control (Ctrl) non-targeting siRNA (A), or cells treated with chloroquine (CQ) or vehicle (Veh) (B). Cells were immunostained for LTβR and EEA1. Insets: Magnified views of boxed regions in the main images. Scale bars, 2 µm.

C   Quantification of a fraction of LTβR signal on the outer membrane of endosomes in cells transfected with siRNAs targeting the indicated ESCRT-I subunits (Tsg101, Vps28), HOPS components or Rab7 (example images in Fig. S6). The fraction is calculated as the ratio of the integral intensity of vesicular LTβR detected by the antibody recognizing its cytoplasmic tail in digitonin- versus saponin-permeabilized cells. Data represent the means ± SEM, n=3. ***P≤0.001 by Mann-Whitney test.

D   Model of the different LTβR topology and signaling upon dysfunction of various trafficking regulators. ESCRT depletion causes LTβR accumulation on the outer membrane of endosomes and activation of NF-κB signaling, while sequestration of LTβR in ILVs upon Rab7/HOPS depletion prevents the transmission of signals to activate the NF-κB pathway.

Figure S1. Depletion of CORVET components does not affect intracellular distribution of LTβR.

A   Immunofluorescence staining of LTβR and EEA1 in HeLa cells upon knockdown of the indicated CORVET components and in control (Ctrl) siRNA-transfected cells. Insets: Magnified views of boxed regions in the main images. Scale bars, 20 μm.

B   Analysis of integral and mean of integral intensities of LTβR-positive vesicles in cells with CORVET knockdown (two independent siRNA oligonucleotides per gene).

C   qRT-PCR analysis of the silencing efficiency of *VPS3* or *VPS8* in HeLa cells.

D   Analysis of colocalization between transferrin and EEA1, and between EGF and EEA1 in cells depleted of Vps3 or Vps8 (as above).

Data information: Black bars (Ctrl_Aver) in B-D represent values averaged of two non-targeting siRNAs transfected independently (Ctrl_1 and Ctrl_2). Data represent the means ± SEM, n=4 (B); n=3 (C, D). ns - P>0.05; *P≤0.05; **P≤0.01 in B and D by ANOVA or Kruskal-Wallis test.
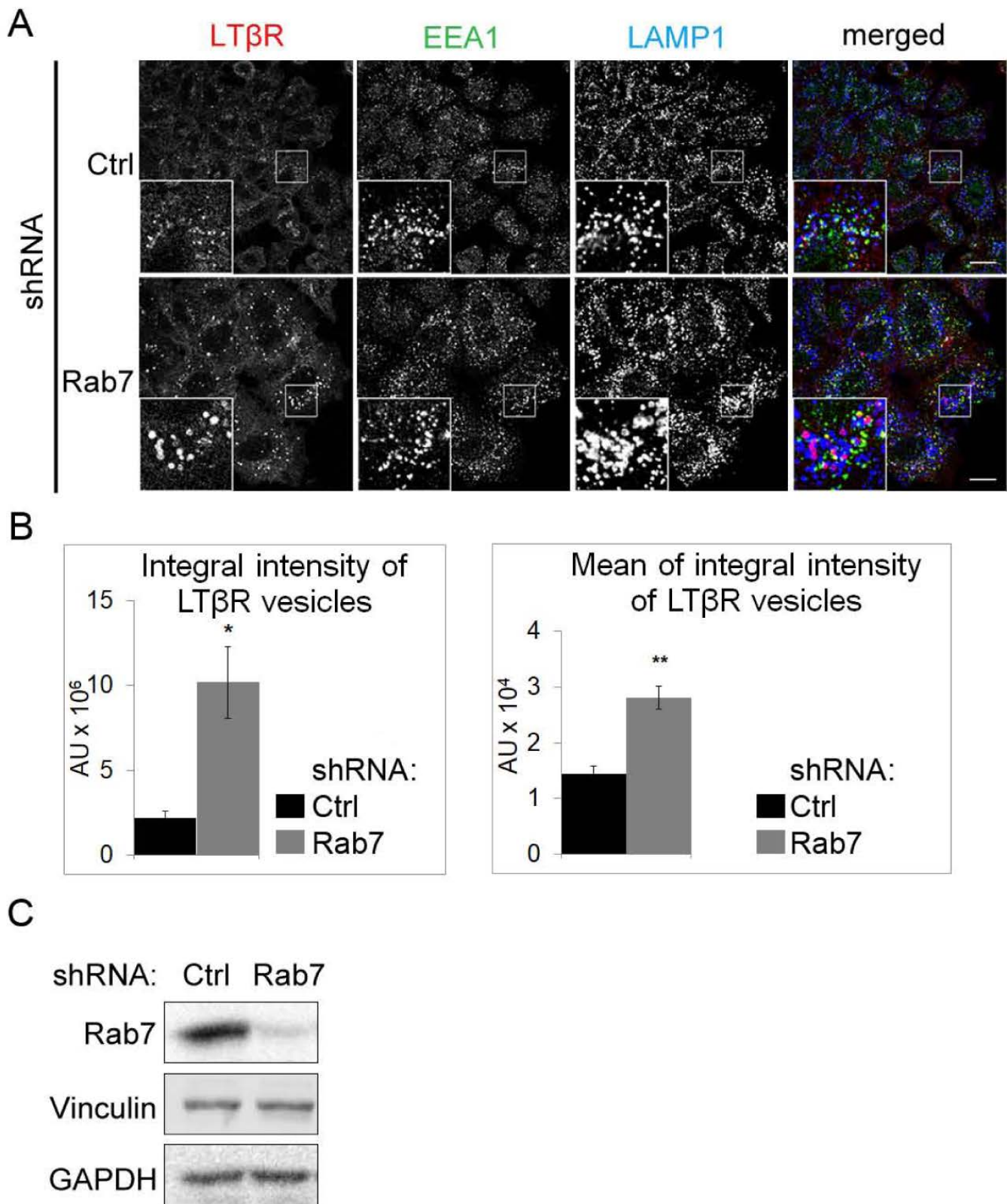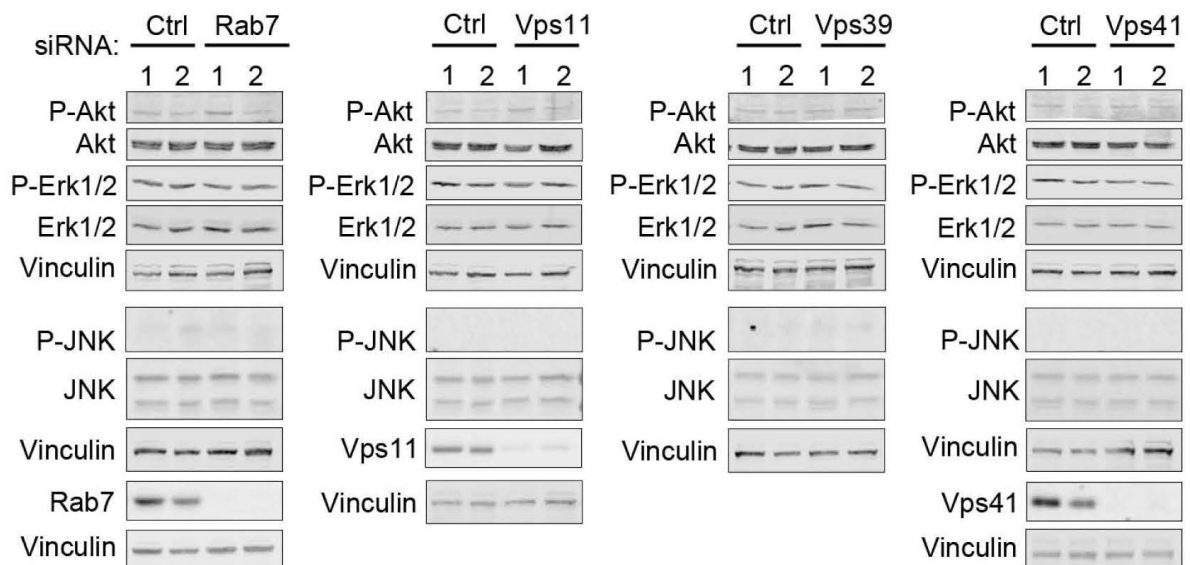
Figure S2. Depletion of HOPS components leads to endosomal accumulation of LTβR.

A   Immunofluorescence staining of LTβR, EEA1 and LAMP1 in HeLa cells upon sgRNA-mediated knockdown of the indicated HOPS components or in parental wildtype (Wt) cells. Insets: Magnified views of boxed regions in the main images. Scale bars, 20 µm.

B   Analysis of integral intensities of EEA1- and LAMP1-positive vesicles in cells with knockdown of Vps39 or Vps41 (two independent sgRNA per gene).

C   Analysis of integral and mean of integral intensities of LTβR-positive vesicles in cells with knockdown of Vps39 or Vps41 (as above).

D   Analysis of colocalization between LTβR, LAMP1 and EEA1; LTβR and EEA1; LTβR and LAMP1 in cells depleted of the indicated HOPS components.

E   qRT-PCR analysis of the silencing efficiency of *VPS39* in HeLa cells.

F   Lysates of HeLa cells depleted of Vps41 by two sgRNAs were analyzed by Western blotting with antibodies against Vps41, with vinculin used as a loading control.

Data information: Black bars (Wt) in B-E represent values of parental Wt HeLa cells. Data represent the means ± SEM, n≥4 (B); n≥4 (C); n=4 (D); n=3 (E). Statistical significance was evaluated using ANOVA test or Kruskal-Wallis test. ns - P>0.05; *P≤0.05; **P≤0.01.

Figure S3. Depletion of Rab7 causes endosomal accumulation of LTβR.

A   Immunofluorescence staining of LTβR, EEA1 and LAMP1 in HeLa cells upon shRNA-mediated knockdown of Rab7 or in control (Ctrl) shRNA-transfected cells. Insets: Magnified views of boxed regions in the main images. Scale bars, 20 μm.

B   Analysis of integral and mean of integral intensities of LTβR-positive vesicles in cells depleted of Rab7 with shRNA.

C   Lysates of HeLa cells depleted of Rab7 with shRNA along with control cells were analyzed by Western blotting with antibodies against Rab7, with GAPDH used as a loading control. Blots are representative of three independent experiments.

Data information: Black bars (Ctrl) in B represent values of non-targeting shRNA sequence. Data represent the means ± SEM, n=3. *P≤0.05;**P≤0.01 by ANOVA test.

Figure S4. Depletion of HOPS components or Rab7 does not affect the status of selected signaling proteins.

A   Quantification of TRAF2 and TRAF3 abundance in HeLa cells depleted of Rab7 (two independent siRNAs) or Vps11 (one siRNA oligonucleotide). TRAF2 and TRAF3 total levels were analyzed by Western blotting (GAPDH was used for normalization) and presented as a fold change versus Ctrl_1, which was assigned a value of 1. Data represent the means ± SEM, n=3.

B, C   Lysates of HeLa cells depleted of Rab7 and HOPS subunits (B) or ESCRT-I subunit Vps28 (C) (two independent siRNAs per gene) were analyzed by Western blotting with antibodies against the indicated signaling proteins (Akt, Erk1/2 and JNK) and against the depleted proteins. Vinculin was used as a loading control. Blots are representative of three experiments.

D   Lysates of HeLa cells treated or not with agonistic anti-LTβR antibody (Ago) were analyzed by Western blotting with the indicated anti-JNK antibodies. Vinculin used as a loading control. Blots are representative of three experiments.

Figure S5. Depletion of HOPS components or Rab7 does not affect the expression of NF-κB target genes.

A, B   qRT-PCR analysis of expression of the indicated NF-κB target genes (*IL8, TNF, ICAM1, NFKBIA, NFKB2, RELB*) in HeLa cells depleted of HOPS components or Rab7 (A) or ESCRT-I component Vps28 (B) with two independent siRNA oligonucleotides per gene and one additional shRNA against Rab7.

C, D   qRT-PCR analysis of expression of the indicated NF-κB target genes in HEK 293 cells depleted of the indicated HOPS components (C) or ESCRT-I component Vps28 (D) with two independent siRNA oligonucleotides per gene.

Expression levels of the indicated NF-κB target genes in A-D are presented as a fold change versus averaged (Ctrl_Aver, black bars) two non-targeting control siRNAs transfected independently (Ctrl_1 and Ctrl_2) or averaged non-targeting shRNA sequence and non-transfected cells in case of Rab7 shRNA (Ctrl_Aver, black bars). Data represent the means ± SEM, n=3 (A); n=4 (B, C, D). ns - P>0.05; *P≤0.05; **P≤0.01; ***P≤0.001 in A (selected genes only: *TNF*, *ICAM1*, *RELB*), B and D by Mann-Whitney, Kruskal-Wallis or ANOVA test.

E   Top Gene Ontology (GO) annotations, according to the DAVID functional annotation tool, among 108 genes identified by microarray analysis as significantly upregulated (FDR<0.05; z-score>0.5) after HOPS depletion in HEK 293 cells. Numbers in brackets indicate gene counts for each annotation.

Figure S6. LTβR localization on endosomes using differential detergent solubilization upon ESCRT or HOPS/Rab7 depletion.

Immunofluorescence staining in HeLa cells upon permeabilization using saponin or digitonin. Cells transfected with siRNAs targeting ESCRT-I (Tsg101,Vps28), HOPS (Vps11, Vps39, Vps41) components or Rab7, and control (Ctrl) siRNA-transfected cells were stained for LTβR with antibodies recognizing the intracellular and extracellular parts of the receptor (mouse and goat antibodies, respectively) and for LAMP1. Quantitative analysis of images is shown in Fig. 6C. Insets: Magnified views of boxed regions in the main images. Scale bars, 20 μm.

Table S1. Sequences of oligonucleotides used for sgRNA cloning

sgRNA name	Sequence	Reference
VPS39-1	Forward: CACCGTTCGGATCTCAACATATCG Reverse: AAACCGATATGTTGAGATCCGAAC	(Doench et al., 2016)
VPS39-2	Forward: CACCGTCTGATTGACTACCTGACAC Reverse: AAACGTGTCAGGTAGTCAATCAGAC	(Doench et al., 2016)
VPS41-1	Forward: CACCGCGAAGACTTATATCATCCCG Reverse: AAACCGGGATGATATAAGTCTTCGC	(Doench et al., 2016)
VPS41-2	Forward: CACCGAGACTATGACATAGCAGCA Reverse: AAACTGCTGCTATGTCATAGTCTC	(Doench et al., 2016)

Table S2. Sequences of primers used for qRT-PCR

Gene name	Forward primer	Reverse primer
ACTB	CAGGTCATCACCATTGGCAAT	TCTTTGCGGATGTCCACGT
B2M	GGAGGCTATCCAGCGTACTC	GAAACCCAGACACATAGCAATTC
IL8	GCTCTCTTGGCAGCCTTCCTGA	TTCCTTGGGGGTCCAGACAGAGC
ICAM1	GGAGCCCGCTGAGGTCACGA	AGTCGCTGGCAGGACAAAGGT
NFKBIA	CGCCCAAGCACCCGGATACA	AGGGCAGCTCGTCCTCTGTGA
NFKB2	GCTGGAGGAGGCGGGCGTCTAA	GGGCTGGCTCCTTGGGTTCCA
RELB	GGAAAGACTGCACCGACGGCA	GGGACCCAGCGTTGTAGGG
TNF	GTGATCGGCCCCCAGAGGGA	T AGGGTTTGCTACAACATGGGC
VPS3	AAGATGCTGCTGCAGTTCAGTTG	TCATACAGGTCTGAGCGTGTGG
VPS8	TGGTGGAGACCATTGCTCTTTGC	AACGGAAACCAAAGTGCCTCAC
VPS16	TCAAGGCTTTGCTTCTTGTTGGC	TGGCCCGTTGAATCTTGTCAGC
VPS18	TCCGAGCGCATTACCAGTCTTG	TGCGGAGCAGTGTATCCTTGC

Table S3. TaqMan® Gene Expression Assays used for qRT-PCR

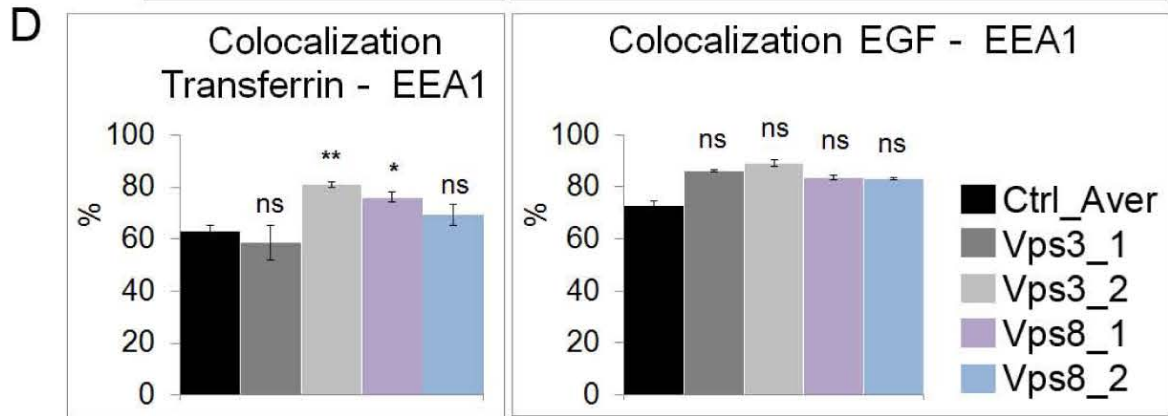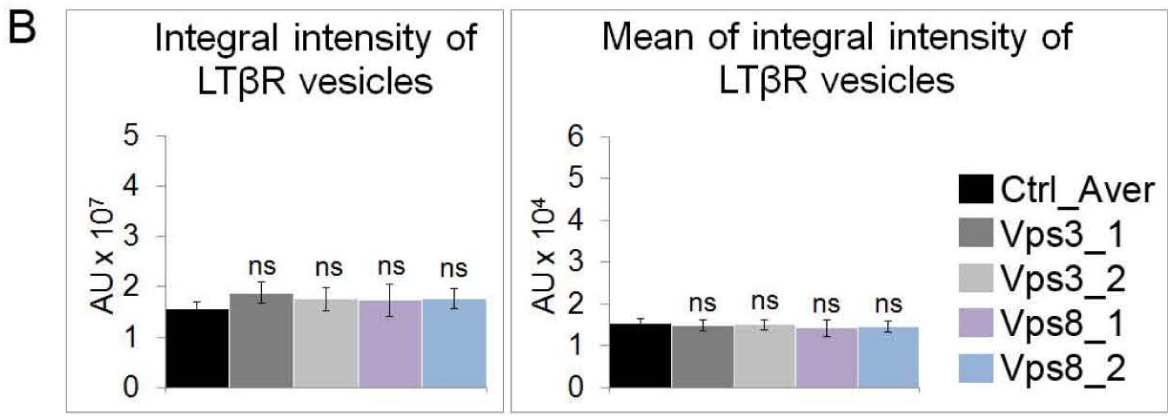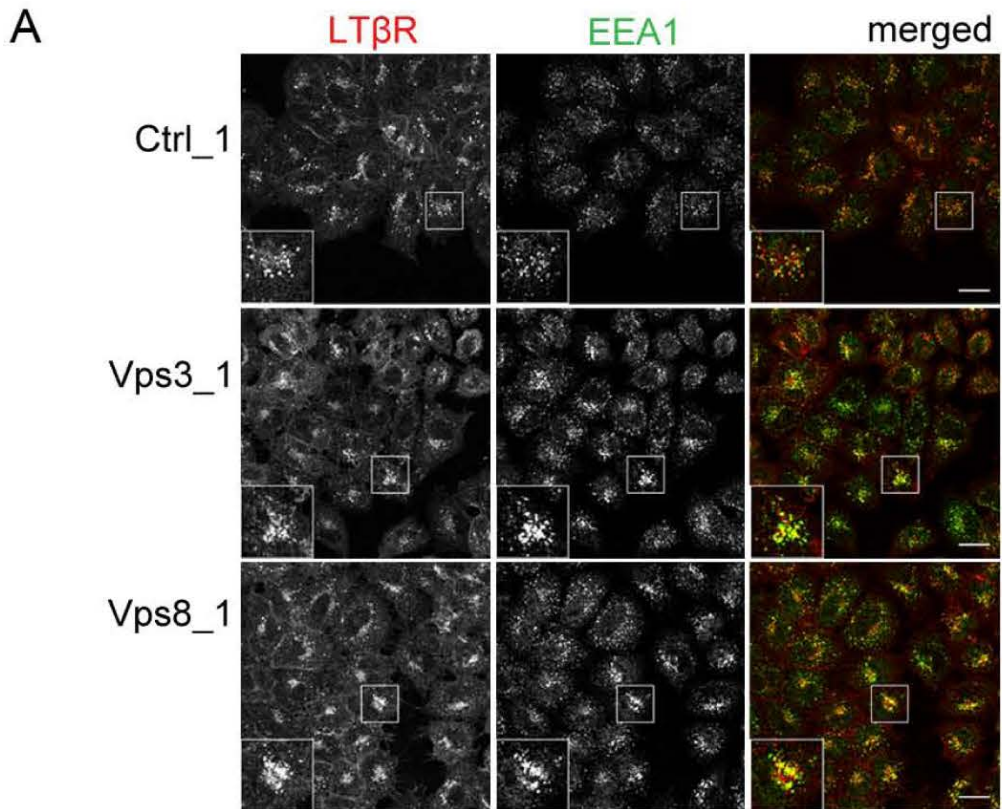| Gene name	TaqMan® Gene Expression Assays
ACTB	Hs99999903_m1
GAPDH	Hs02758991_g1
VPS11	Hs00222240_m1
VPS39	Hs00385779_m1
VPS41	Hs00205216_m1

Figure S1. Depletion of CORVET components does not affect intracellular distribution of LTβR.

A   Immunofluorescence staining of LTβR and EEA1 in HeLa cells upon knockdown of the indicated CORVET components and in control (Ctrl) siRNA-transfected cells. Insets: Magnified views of boxed regions in the main images. Scale bars, 20 μm.

B   Analysis of integral and mean of integral intensities of LTβR-positive vesicles in cells with CORVET knockdown (two independent siRNA oligonucleotides per gene).

C   qRT-PCR analysis of the silencing efficiency of *VPS3* or *VPS8* in HeLa cells.

D   Analysis of colocalization between transferrin and EEA1, and between EGF and EEA1 in cells depleted of Vps3 or Vps8 (as above).

Data information: Black bars (Ctrl_Aver) in B-D represent values averaged of two non-targeting siRNAs transfected independently (Ctrl_1 and Ctrl_2). Data represent the means ± SEM, n=4 (B); n=3 (C, D). ns - P>0.05; *P≤0.05; **P≤0.01 in B and D by ANOVA or Kruskal-Wallis test.
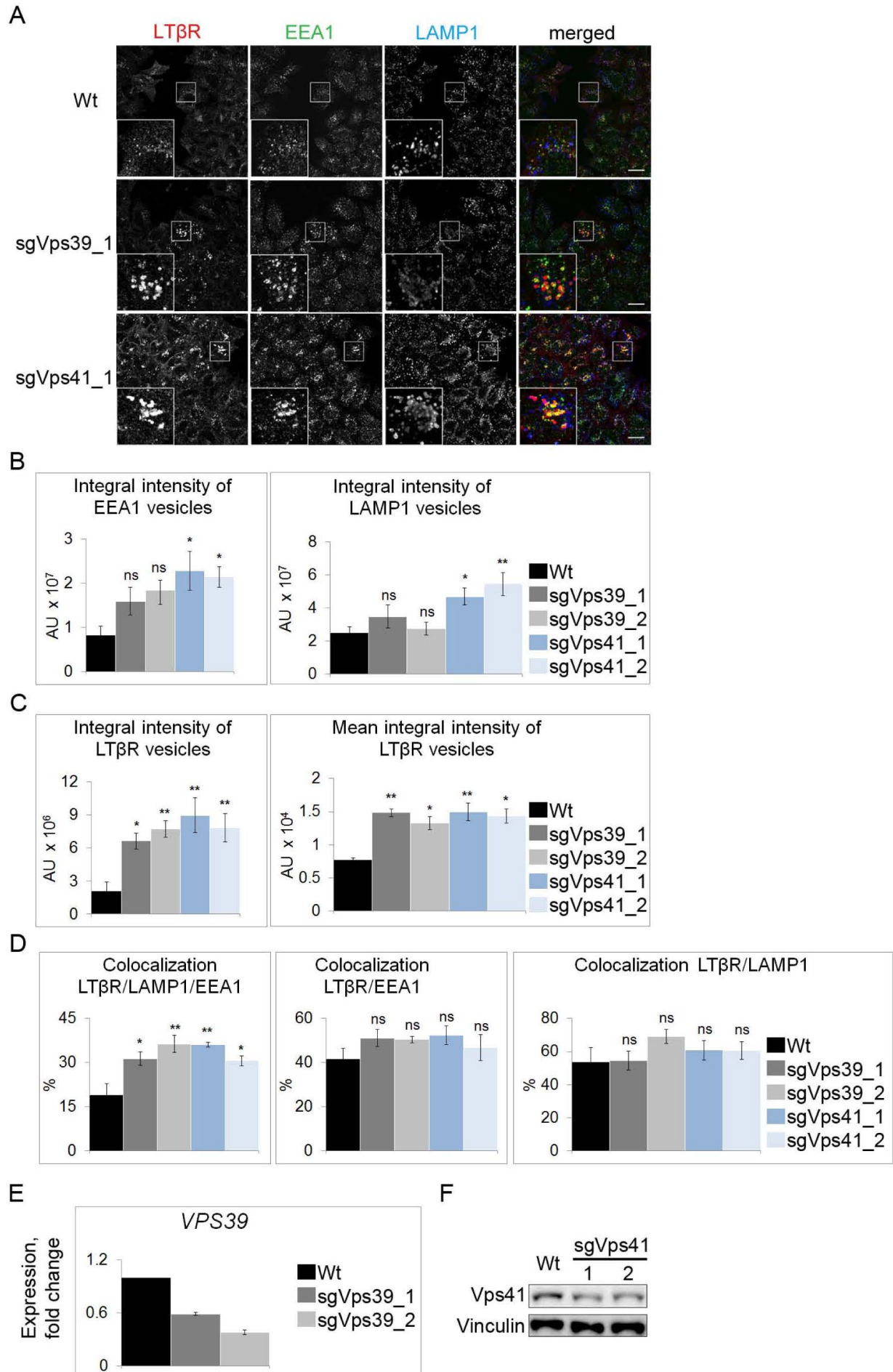
Figure S2. Depletion of HOPS components leads to endosomal accumulation of LTβR.

A   Immunofluorescence staining of LTβR, EEA1 and LAMP1 in HeLa cells upon sgRNA-mediated knockdown of the indicated HOPS components or in parental wildtype (Wt) cells. Insets: Magnified views of boxed regions in the main images. Scale bars, 20 μm.

B   Analysis of integral intensities of EEA1- and LAMP1-positive vesicles in cells with knockdown of Vps39 or Vps41 (two independent sgRNA per gene).

C   Analysis of integral and mean of integral intensities of LTβR-positive vesicles in cells with knockdown of Vps39 or Vps41 (as above).

D   Analysis of colocalization between LTβR, LAMP1 and EEA1; LTβR and EEA1; LTβR and LAMP1 in cells depleted of the indicated HOPS components.

E   qRT-PCR analysis of the silencing efficiency of *VPS39* in HeLa cells.

F   Lysates of HeLa cells depleted of Vps41 by two sgRNAs were analyzed by Western blotting with antibodies against Vps41, with vinculin used as a loading control.

Data information: Black bars (Wt) in B-E represent values of parental Wt HeLa cells. Data represent the means ± SEM, n≥4 (B); n≥4 (C); n=4 (D); n=3 (E). Statistical significance was evaluated using ANOVA test or Kruskal-Wallis test. ns - P>0.05; *P≤0.05; **P≤0.01.
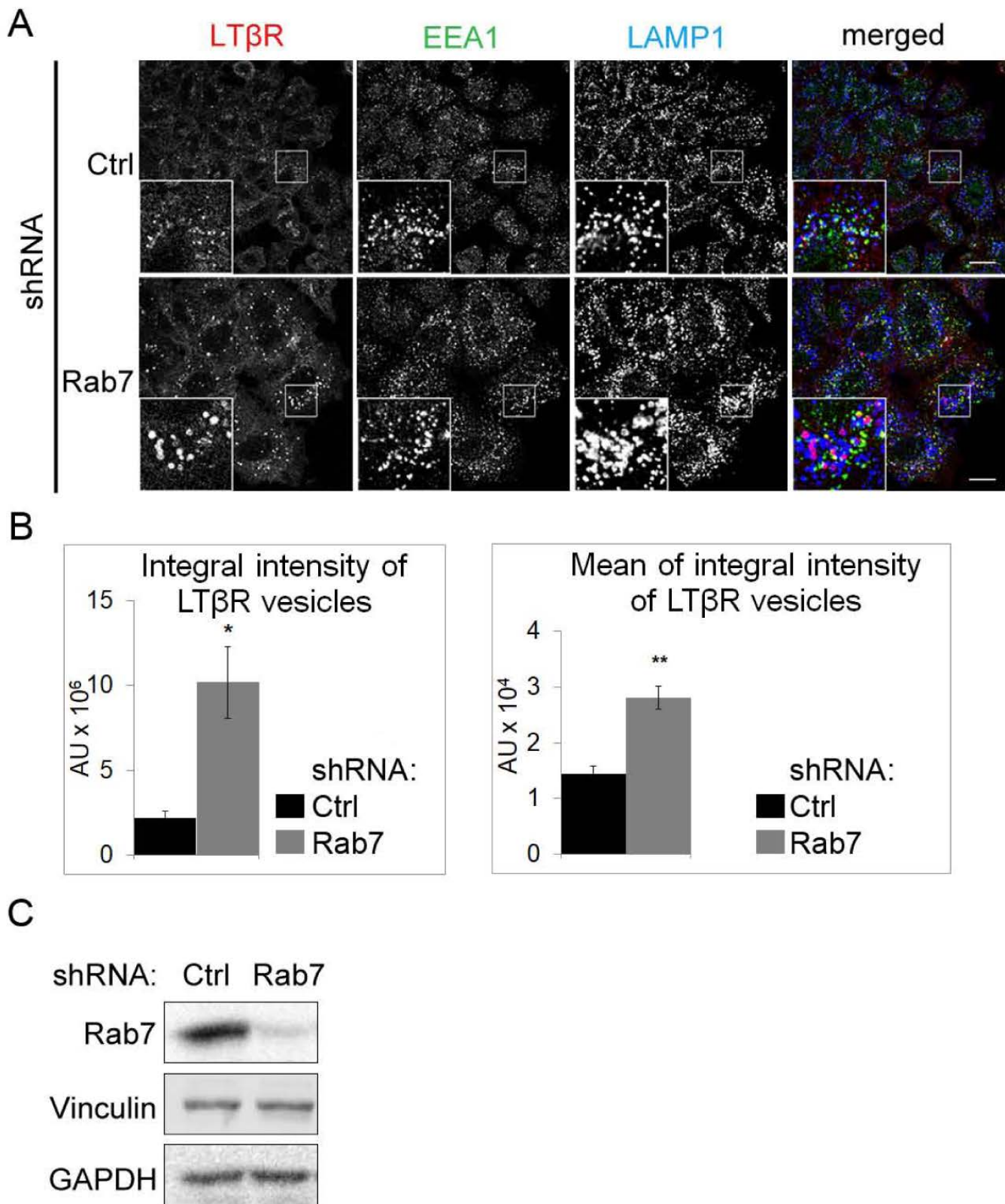
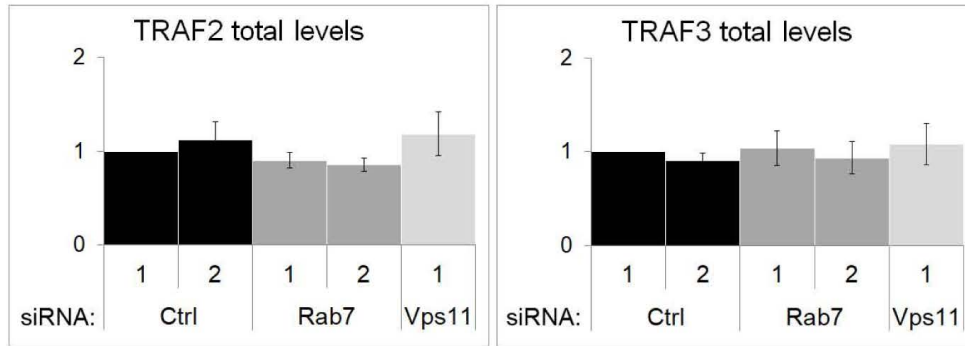**Figure S3. Depletion of Rab7 causes endosomal accumulation of LTβR.**

A   Immunofluorescence staining of LTβR, EEA1 and LAMP1 in HeLa cells upon shRNA-mediated knockdown of Rab7 or in control (Ctrl) shRNA-transfected cells. Insets: Magnified views of boxed regions in the main images. Scale bars, 20 μm.

B   Analysis of integral and mean of integral intensities of LTβR-positive vesicles in cells depleted of Rab7 with shRNA.
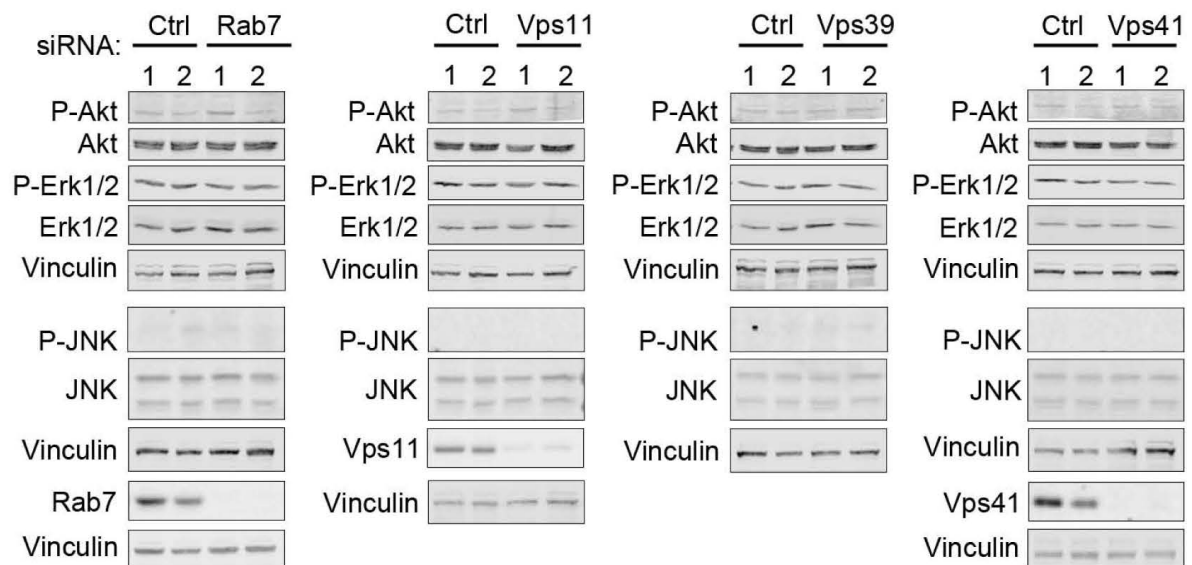
C   Lysates of HeLa cells depleted of Rab7 with shRNA along with control cells were analyzed by Western blotting with antibodies against Rab7, with GAPDH used as a loading control. Blots are representative of three independent experiments.

Data information: Black bars (Ctrl) in B represent values of non-targeting shRNA sequence. Data represent the means ± SEM, n=3. *P≤0.05;**P≤0.01 by ANOVA test.
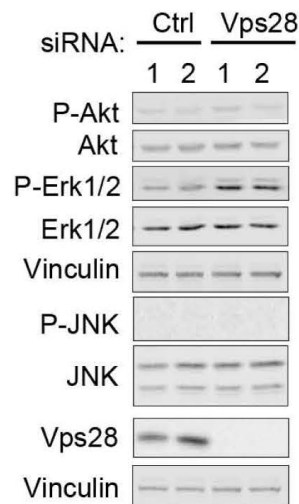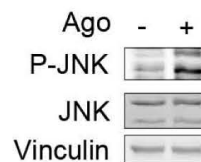
Figure S4. Depletion of HOPS components or Rab7 does not affect the status of selected signaling proteins.

A   Quantification of TRAF2 and TRAF3 abundance in HeLa cells depleted of Rab7 (two independent siRNAs) or Vps11 (one siRNA oligonucleotide). TRAF2 and TRAF3 total levels were analyzed by Western blotting (GAPDH was used for normalization) and presented as a fold change versus Ctrl_1, which was assigned a value of 1. Data represent the means ± SEM, n=3.

B, C   Lysates of HeLa cells depleted of Rab7 and HOPS subunits (B) or ESCRT-I subunit Vps28 (C) (two independent siRNAs per gene) were analyzed by Western blotting with antibodies against the indicated signaling proteins (Akt, Erk1/2 and JNK) and against the depleted proteins. Vinculin was used as a loading control. Blots are representative of three experiments.

D   Lysates of HeLa cells treated or not with agonistic anti-LTβR antibody (Ago) were analyzed by Western blotting with the indicated anti-JNK antibodies. Vinculin used as a loading control. Blots are representative of three experiments.
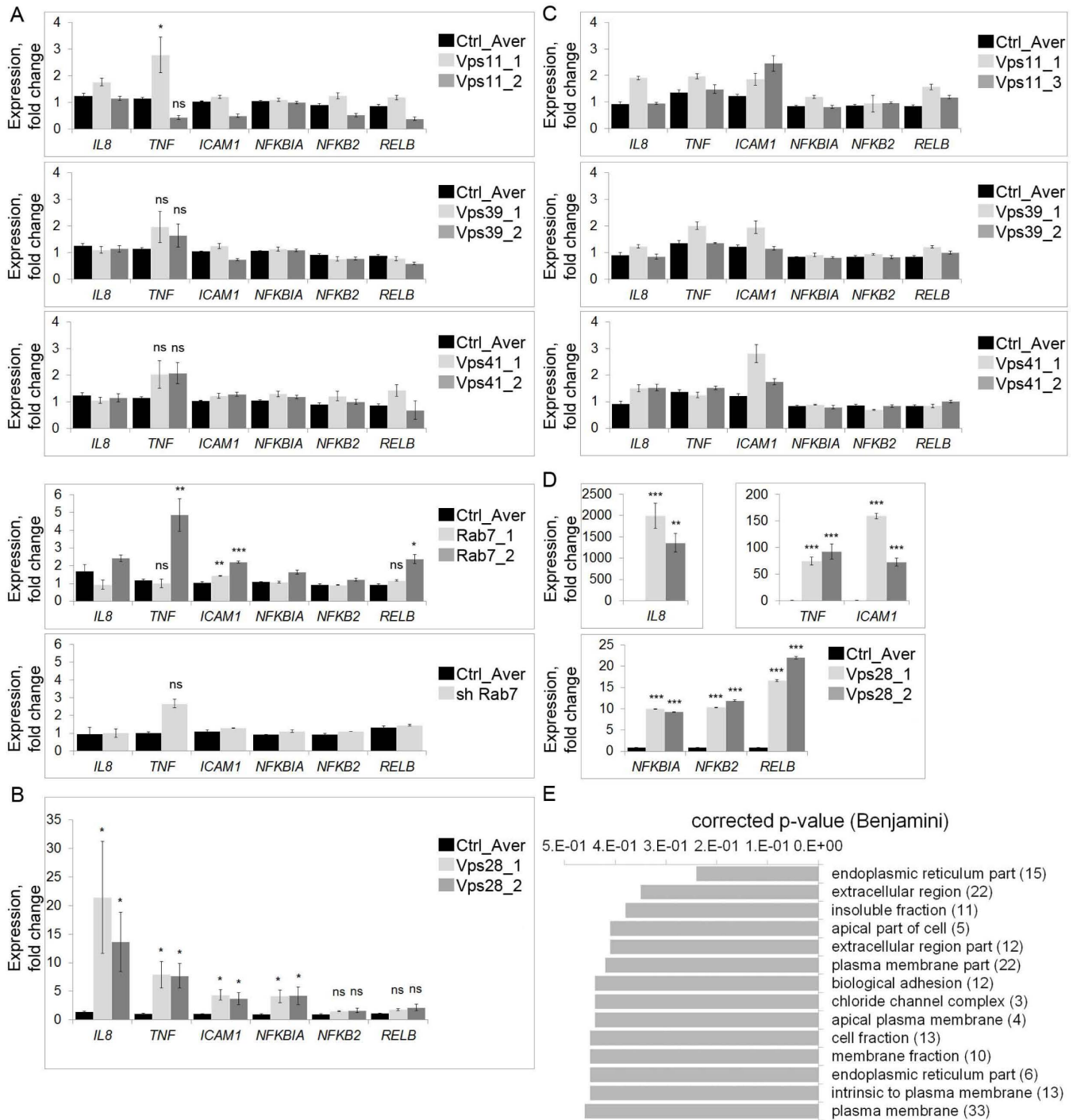
Figure S5. Depletion of HOPS components or Rab7 does not affect the expression of NF-κB target genes.

A, B   qRT-PCR analysis of expression of the indicated NF-κB target genes (*IL8, TNF, ICAM1, NFKBIA, NFKB2, RELB*) in HeLa cells depleted of HOPS components or Rab7 (A) or ESCRT-I component Vps28 (B) with two independent siRNA oligonucleotides per gene and one additional shRNA against Rab7.

C, D   qRT-PCR analysis of expression of the indicated NF-κB target genes in HEK 293 cells depleted of the indicated HOPS components (C) or ESCRT-I component Vps28 (D) with two independent siRNA oligonucleotides per gene.

Expression levels of the indicated NF-κB target genes in A-D are presented as a fold change versus averaged (Ctrl_Aver, black bars) two non-targeting control siRNAs transfected independently (Ctrl_1 and Ctrl_2) or averaged non-targeting shRNA sequence and non-transfected cells in case of Rab7 shRNA (Ctrl_Aver, black bars). Data represent the means ± SEM, n=3 (A); n=4 (B, C, D). ns - P>0.05; *P≤0.05; **P≤0.01; ***P≤0.001 in A (selected genes only: *TNF*, *ICAM1*, *RELB*), B and D by Mann-Whitney, Kruskal-Wallis or ANOVA test.

E   Top Gene Ontology (GO) annotations, according to the DAVID functional annotation tool, among 108 genes identified by microarray analysis as significantly upregulated (FDR<0.05; z-score>0.5) after HOPS depletion in HEK 293 cells. Numbers in brackets indicate gene counts for each annotation.
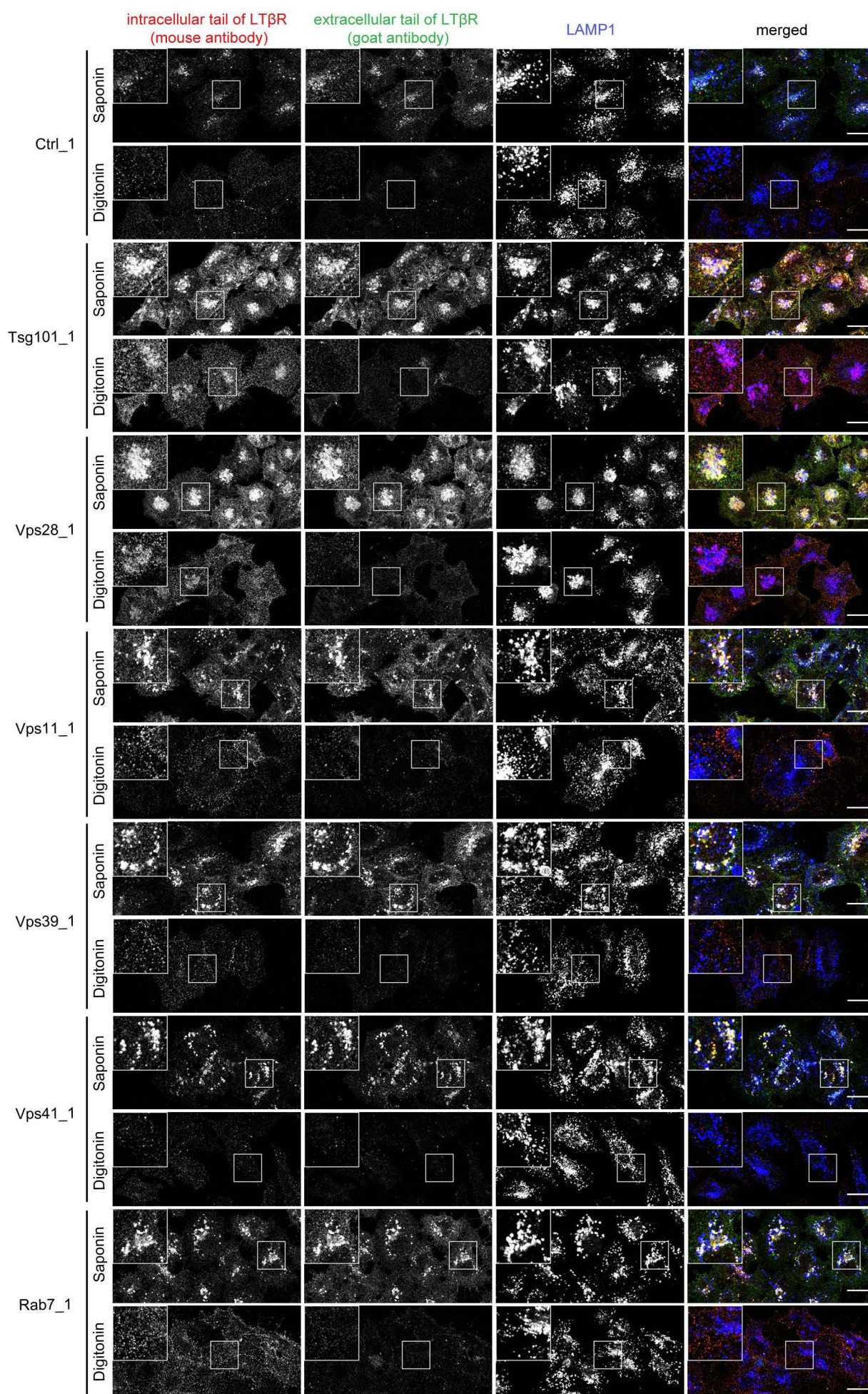
Figure S6. LTβR localization on endosomes using differential detergent solubilization upon ESCRT or HOPS/Rab7 depletion.

Immunofluorescence staining in HeLa cells upon permeabilization using saponin or digitonin. Cells transfected with siRNAs targeting ESCRT-I (Tsg101,Vps28), HOPS (Vps11, Vps39, Vps41) components or Rab7, and control (Ctrl) siRNA-transfected cells were stained for LTβR with antibodies recognizing the intracellular and extracellular parts of the receptor (mouse and goat antibodies, respectively) and for LAMP1. Quantitative analysis of images is shown in Fig. 6C. Insets: Magnified views of boxed regions in the main images. Scale bars, 20 μm.

Table S1. Sequences of oligonucleotides used for sgRNA cloning

sgRNA name	Sequence	Reference
VPS39-1	Forward: CACCGTTCGGATCTCAACATATCG Reverse: AAACCGATATGTTGAGATCCGAAC	(Doench et al., 2016)
VPS39-2	Forward: CACCGTCTGATTGACTACCTGACAC Reverse: AAACGTGTCAGGTAGTCAATCAGAC	(Doench et al., 2016)
VPS41-1	Forward: CACCGCGAAGACTTATATCATCCCG Reverse: AAACCGGGATGATATAAGTCTTCGC	(Doench et al., 2016)
VPS41-2	Forward: CACCGAGACTATGACATAGCAGCA Reverse: AAACTGCTGCTATGTCATAGTCTC	(Doench et al., 2016)

Table S2. Sequences of primers used for qRT-PCR

Gene name	Forward primer	Reverse primer
ACTB	CAGGTCATCACCATTGGCAAT	TCTTTGCGGATGTCCACGT
B2M	GGAGGCTATCCAGCGTACTC	GAAACCCAGACACATAGCAATTC
IL8	GCTCTCTTGGCAGCCTTCCTGA	TTCCTTGGGGGTCCAGACAGAGC
ICAM1	GGAGCCCGCTGAGGTCACGA	AGTCGCTGGCAGGACAAAGGT
NFKBIA	CGCCCAAGCACCCGGATACA	AGGGCAGCTCGTCCTCTGTGA
NFKB2	GCTGGAGGAGGCGGGCGTCTAA	GGGCTGGCTCCTTGGGTTCCA
RELB	GGAAAGACTGCACCGACGGCA	GGGACCCAGCGTTGTAGGG
TNF	GTGATCGGCCCCCAGAGGGA	T AGGGTTTGCTACAACATGGGC
VPS3	AAGATGCTGCTGCAGTTCAGTTG	TCATACAGGTCTGAGCGTGTGG
VPS8	TGGTGGAGACCATTGCTCTTTGC	AACGGAAACCAAAGTGCCTCAC
VPS16	TCAAGGCTTTGCTTCTTGTTGGC	TGGCCCGTTGAATCTTGTCAGC
VPS18	TCCGAGCGCATTACCAGTCTTG	TGCGGAGCAGTGTATCCTTGC

Table S3. TaqMan® Gene Expression Assays used for qRT-PCR

Gene name	TaqMan® Gene Expression Assays
ACTB	Hs99999903_m1
GAPDH	Hs02758991_g1
VPS11	Hs00222240_m1
VPS39	Hs00385779_m1
VPS41	Hs00205216_m1